Author/s:
Ryan, E;Nguyen, CQN;Shiea, C;Reid, GE

Title:
Detailed Structural Characterization of Sphingolipids via 193 nm Ultraviolet Photodissociation and Ultra High Resolution Tandem Mass Spectrometry

Date:
2017-07-01

Citation:
Ryan, E., Nguyen, C. Q. N., Shiea, C. & Reid, G. E. (2017). Detailed Structural Characterization of Sphingolipids via 193 nm Ultraviolet Photodissociation and Ultra High Resolution Tandem Mass Spectrometry. Journal of the American Society for Mass Spectrometry, 28 (7), pp.1406-1419. https://doi.org/10.1007/s13361-017-1668-1.

Persistent Link:
https://hdl.handle.net/11343/283161

Detailed Structural Characterization of Sphingolipids via 193 nm Ultraviolet Photodissociation and Ultra High Resolution Tandem Mass Spectrometry

Eileen Ryan[1], Catherine Quynh Nguyen[1], Christopher Shiea[1] and Gavin E. Reid[1,2,3*]

[1]School of Chemistry, [2]Department of Biochemistry and Molecular Biology, [3]Bio21 Molecular Science and Biotechnology Institute. University of Melbourne, Parkville, Victoria 3010, Australia

*Address Correspondence to: gavin.reid@unimelb.edu.au

Keywords: lipidomics, photodissociation, unsaturation, high resolution mass spectrometry, sphingolipid

Abstract

Sphingolipids serve not only as components of cellular membranes but also as bioactive mediators of numerous cellular functions. As the biological activities of these lipids are dependent on their structures, and due to the limitations of conventional ion activation methods employed during tandem mass spectrometry (MS/MS), there is a recognized need for the development of improved structure-specific methods for their comprehensive identification and characterization. Here, positive-ionization mode 193 nm ultraviolet photodissociation (UVPD)-MS/MS has been implemented for the detailed structural characterization of lipid species from a range of sphingolipid classes introduced to the mass spectrometer via electrospray ionization as their lithiated or protonated adducts. These include sphingosine d18:1(4E), dihydrosphingosine (sphinganine) d18:0, sphingadiene d18:2(4E,11Z), the isomeric sphingolipids ceramide d18:1(4E)/18:0 and dihydroceramide d18:0/18:1(9Z), ceramide-1-phosphate d18:1(4Z)/16:0, sphingomyelin d18:1(4E)/18:1(9Z) the glycosphingolipids galactosyl ceramide d18:1(4E)/24:1(15Z) and lactosyl ceramide d18:1(4E)/24:0, and several endogenous lipids present within a porcine brain total lipid extract. In addition to the product ions formed by higher energy collision dissociation (HCD), UVPD is shown to yield a series of novel structurally diagnostic product ions resulting from cleavage of both sphingosine carbon-carbon and acyl chain carbon-carbon double bonds for direct localization of site(s) of unsaturation, as well as via diagnostic cleavages of the sphingosine backbone and N-C amide bond linkages. With activation timescales and dissociation efficiencies similar to those found in conventional MS/MS strategies, this approach is therefore a promising new tool in the arsenal of ion activation techniques toward providing complete structural elucidation in automated, high-throughput lipid analysis workflows.

Introduction

Sphingolipids represent one of the eight major structurally distinct categories of lipids [1]. Sphingolipids are ubiquitous in all eukaryotic cells and play important structural roles in regulation of the fluidity and subdomain structure of lipid bilayers [2], and as bioactive regulators of cellular proliferation, differentiation, cell migration, cell signalling, autophagy and cell death [3]. The involvement of sphingolipids in a diverse range of cellular processes has implications for the understanding of cancer biology, arthritis, inflammation, diabetes, immune function and neurodegenerative disorders [3-5]. Not surprisingly, therefore, there is a recognised need for effective methods that enable qualitative and quantitative profiling of the diverse range of sphingolipids that may be present within complex lipid matrices, i.e., 'sphingolipidomics', under different physiological or pathological conditions. Importantly, the physiochemical properties and biological functions of sphingolipids are dependent on their individual structures, whereby seemingly simple alterations involving the absence, presence, or site specific location of a double bond within the sphingoid backbone or acyl chain components can have a profound impact [6]. Thus, sphingolipidomic studies that aim to comprehensively determine the functional role of sphingolipids must endeavour to ultimately characterize the entire ensemble of 'structurally defined molecular lipid' [7] species that are present, including (i) the identity and chain length of the sphingoid base i.e., sphingosine versus dihydrosphingosine (sphinganine) (ii) the chain length of any amide-linked acyl groups, (iii) the number, locations and diasteromeric configurations of any sites of unsaturation within the acyl and/or sphingoid chains, and (iv) the identity of any headgroups that are present [8].

Electrospray ionization-mass spectrometry (ESI-MS), coupled with tandem mass spectrometry (MS/MS) for structural elucidation, has emerged as the key enabling platform technology for lipidomics [9-11]. However, the sphingolipidome can potentially be

comprised of tens of thousands of discrete molecular species, many of which are isomeric, thereby making their comprehensive identification and characterization a significant analytical challenge [8,12]. Conventional MS/MS-based structural elucidation methods employing low-energy collision-induced dissociation (CID) or higher collision-energy dissociation (HCD) can provide information about the overall length and total number of double bonds that comprise the sphingoid base and the amide-linked acyl chain, as well as the identity of the headgroup [10-14]. However, molecular species-specific information to confirm the identity of the sphingoid base (i.e., sphingosine vs. an unsaturated dihydrosphingosine), and the site specific locations and diasteromeric configurations of any sites of unsaturation within the sphingoid base or amide-linked acyl chains, are typically not obtained. Indeed, this is a general limitation for all classes of lipids when using low energy collisional activation MS/MS methods.

Several strategies have been developed and applied to overcome some of these deficiencies. These include the use of multistage tandem mass spectrometry (i.e., CID-MS^3) on the lithiated adducts of unsaturated glycerophospholipids and triacylglyceride ions [15,16], or by performing low energy CID-MS/MS on unsaturated fatty acid ions subjected to 'charge switch' derivatization [17], that each yield product ions indicative of the location of C=C double bonds within these species. More recently, the initial products formed by photochemical Paternò-Büchi reaction occurring within a nanoelectrospray ionization (nanoESI) plume (i.e., a [2+2] cycloaddition reaction that results in highly specific modification of the C=C double bonds within unsaturated lipids, where acetone is used as the reagent under 254-nm UV irradiation conditions) have been shown to subsequently dissociate under low energy CID-MS/MS conditions to yield abundant carbon-carbon double bond specific product ions for locating C=C isomers within unsaturated fatty acids and glycerophospholipid species [18]. This approach has subsequently been applied to reveal

significant changes in the ratios of these isomers between normal and cancerous tissues [19]. Similarly, in a technique termed radical-directed dissociation (RDD), radical product ions are formed by 266 nm irradiation of a mass selected unsaturated lipid precursor ion complexed covalently or non-covalently with a molecule containing a photocaged radical initiator, via selective cleavage of a carbon–iodine bond. Upon further mass selection, these products undergo subsequent low energy CID-MS/MS to yield characteristic fragments that are diagnostic for the double bond position and the positions of chain-branching in glycerophospholipids, sphingomyelins and triacylglycerols [20,21]. This approach has also been recently applied to the differentiation of glucosyl versus galactosyl epimers of various glycosphingolipid ions [22].

The elucidation of double bond positions in unsaturated lipids can also be achieved directly via a gas-phase ion-molecule reaction between mass selected unsaturated lipid precursor ions and ozone (i.e., the well-established ozone-induced dissociation (OzID) technique) [23,24], whose unstable initial product decomposes to yield a pair of product ions that are diagnostic for the location of each carbon-carbon double bond that is present within the molecule. Importantly, by performing sequential CID and OzID, whereby the initial product ions arising from CID are isolated and then subjected to ozonolysis, additional information regarding the sn-positions of acyl substituents on the glycerol backbone of phospholipid ions can also be obtained [25].

As an alternative to collisional activation, electron-induced dissociation (EID) [26] and electron impact excitation of ions from organics (EIEIO) [27] have both been recently applied toward the identification of lipid class, and localization of acyl chains and double-bond positions within glycerophosphatidylcholine lipids, as well as for sphingolipid molecular species [28]. Finally, Penning ionization of the singly charged precursor ions of phospholipid cations to their respective radical dications, using He-metastable atom-activated

dissociation (He-MAD), has been reported to induce fragmentations consistent with those formed via high-energy collision induced dissociation, including product ions corresponding to cleavage at or near the double bond position [29].

Each of the techniques described above have their own strengths, but, depending on the technique, can potentially be limited by their necessity for specialized instrumentation, added mixture complexity due to incomplete reaction of non-mass selected precursor ions, or relatively poor signal-to-noise levels within the product ion spectrum due to limited dissociation efficiencies or 'dilution' of the spectrum when the double bond is localised by the absence of a fragmentation within a series of non-specific fragmentations along the acyl chain.

Over the past decade, there has been increasing interest in the potential for ultraviolet photodissociation (UVPD) as an ion activation method that is independent or complementary to CID for direct dissociation, characterization and isomer differentiation of a range of biomolecular species including peptides, proteins and lipids [30]. To date, 157 nm [31] and 193 nm [32-34] wavelengths have been reported for UPVD-MS/MS structural characterization of lipids. For example, it was demonstrated that isomeric leukotrienes, i.e., bioactive inflammatory lipid mediators produced by the enzymatic oxidation of arachidonic acid (AA) and eicosapentaenoic acid (EPA, can be diff erentiated by using 157 nm UVPD, which results in the formation of specific diagnostic radical ions [31]. Brodbelt and colleagues have demonstrated the benefits of negative ionization mode 193 nm UVPD-MS/MS for the characterization of lipid A (typically composed of a bisphosphorylated diglucosamine with a variable number of amide and ester-linked fatty acid chains) structures, including assignment of acyl chain C-O, C-N, and C-C bond cleavages and glycosidic C-O and cross ring cleavages [32-34], as well as other rough-type lipopolysaccharides [35]. O'Brien and Brodbelt also reported the novel use of 193 nm UVPD for the improved

structural characterization of various glycosphingolipids and gangliosides in negative-ionization mode, including the observation of several types of diagnostic fragment ions including glycosidic cross-ring cleavages and C-C and C-N bond cleavages at the sphingosine and fatty acid moieties, that are not observed using conventional collisional activation MS/MS methods [36].

To date, there has been only one report of 193 nm UVPD-MS/MS for lipid structural analysis in positive-ionization mode [37]. In this recent report, Klein and Brodbelt demonstrated that UVPD of protonated glycerophosphatidylcholine (PC) lipid ions resulted in cleavage of the carbon-carbon bonds adjacent to double bonds located within their acyl chains, providing a diagnostic mass difference of 24 Da, and thereby enabling localization of the double bond positions and differentiation of double-bond positional isomers. Herein, to further explore the photodissociation behavior of lipid ions in the gas-phase, we report the first study of positive-ionization mode 193 nm UVPD-MS/MS combined with ultra-high resolution mass spectrometry for the structural characterisation of several major classes of sphingolipids (**Scheme 1**), including sphingosine, dihydrosphingosine (sphinganine), sphingadiene, ceramide, ceramide-1-phosphate, sphingomyelin, galactosyl ceramide and lactosyl ceramide, as well as several endogenous sphingolipids present within a total lipid extract of porcine brain.

<insert Scheme 1 here>

Experimental

Materials

Sphingosine d18:1(4E), dihydrosphingosine d18:0, sphingadiene d18:2(4E,11Z), ceramide d18:1(4E)/18:0, dihydroceramide d18:0/18:1(9Z), ceramide-1-phosphate d18:1(4E)/16:0, sphingomyelin d18:1(4E)/18:1(9Z), galactosyl ceramide d18:1(4E)/24:1(15Z), lactosyl ceramide d18:1(4E)/24:0 and porcine brain total lipid extract were purchased as powders from Avanti Polar Lipids, Inc. (Alabaster, AL). Isopropanol, methanol, and chloroform (high performance liquid chromatography grade) were from Fisher Scientific (Waltham, MA). Lithium acetate was from SigmaAldrich (St. Louis, MO).

Sample Preparation

Solutions of individual lipid standards (10 µM) were prepared by placing 10 µL of 100 µM individual lipid standards dissolved in chloroform into the wells of an Eppendorf twin-tec 96-well PCR plate, dried down under nitrogen, then resuspended in 100 µL isopropanol : methanol : chloroform (4:2:1, v:v:v) containing 2 mM lithium acetate (i.e., a final concentration of 10 µM). The porcine brain total lipid extract was prepared at a concentration of 50 µg/mL in isopropanol : methanol : chloroform (4:2:1, v:v:v) containing 2 mM lithium acetate then placed into the wells of an Eppendorf twin-tec 96-well PCR plate. The plates were then sealed with Teflon Ultra-Thin Sealing Tape (Analytical Sales and Services, Pompton Plains, NJ) prior to MS analysis.

Modification of a Q Exactive Orbitrap Mass Spectrometer to perform 193 nm UVPD

193 nm UVPD MS/MS was implemented on a Q Exactive Orbitrap mass spectrometer (Thermo Fisher Scientific, Bremen, Germany), similar to that recently described

by Fort *et al*. [38]. A CaF_2 optical window was introduced into the rear access port of the vacuum manifold. After removal of the electrometer positioned at the exit of the HCD cell, the output from a Coherent ExciStar XS ArF excimer laser (Santa Clara, CA) (8 mJ energy max., up to 500 Hz rep. rate, 2.5 W Average Pulse Power, 5 ns pulse duration) was directed coaxially (but slightly off-axis to reduce the formation of low m/z photon-induced ions resulting from the photons hitting the C-trap assembly) into the HCD cell using standard UV optics. Collimation of the laser pulses was achieved using an aperture plate with a 2.0 mm central hole mounted inside vacuum manifold between the optical window and the HCD cell. The laser was triggered by using the output from the split lens of the mass spectrometer. Control over the ion trapping time, and the HCD collision energy (i.e., below the default value of 10% NCE), was achieved using custom software patches within the mass spectrometer control software. Optimization of the temporal overlap between the ion packets and the photons, and control of the number of laser shots and the delay between shots within a given UVPD activation period, was controlled using a Berkeley Nucleonics Corporation (San Rafael, CA) model 505 Pulse generator. Importantly, the normal function and performance of the mass spectrometer was not altered by these modifications.

Mass Spectrometry

Samples were introduced to the mass spectrometer via nanoESI (nESI) using an Advion Triversa Nanomate (Advion, Ithaca, NY) operating at a spray voltage of 1.2 kV and a gas pressure of 0.3 psi. The ion source interface settings (inlet temperature of 200°C and S-Lens value of 50%) were optimized to maximize the sensitivity of the precursor ions while minimizing 'in-source' fragmentation. All nESI-MS/MS spectra were acquired in the Orbitrap mass analyser using a mass resolving power of 70,000 (at m/z 400). The AGC target was maintained at 5×10^5 and the maximum ion injection time was set to 500 ms. Precursor

ions were monoisotopically isolated using an isolation window of ± 0.2 m/z. UVPD spectra were generated using 5 to 40 laser pulses/scan, depending on the lipid species, during which the HCD collision energy was set to 2 eV. For HCD-MS/MS, the collision energies were individually optimized to provide similar dissociation efficiencies to those observed for each UVPD experiment. Spectra shown are the average of 100 scans in order to provide high signal-to-noise ratios for the initial structural assignments. However, the average of only 3-5 scans was found to provide sufficient signal-to-noise for practical applications.

Results and Discussion

193 nm UVPD- and HCD-MS/MS of Sphingoid Bases

Sphingoid bases or long-chain bases (LCB) are the fundamental building blocks of all sphingolipids, consisting of 2-amino-1,3-dihydroxy-alkanes or alkenes with variable alkyl chain lengths. Over sixty different species of LCBs have been reported, with alkyl chain lengths containing 14 to 22 carbons, and with the possibility of containing double bonds in addition to that at the C4-position within sphingosine lipids [12,39,40]. However, in mammalians, the main sphingoid bases are the C18 sphingosine and dihydrosphingosine (sphinganine) derivatives (**Scheme 1**).

Initially, to compare the photodissociation and collisional activation fragmentation behavior of these simplest of sphingolipids, 193 nm UVPD and HCD-MS/MS spectra were acquired for the $[M+Li]^+$ adducts of sphingosine d18:1(4E) (m/z 306.2976) (**Figure 1A** and **1B**, respectively), and dihydrosphingosine d18:0 (m/z 308.3130) (**Supplemental Figure S1A** and **S1B**, respectively). For the sphingosine ion, UVPD was observed to generally yield the same products as HCD i.e., cleavage of the alkyl chain at the C2-C3 position to form m/z 245.2499 and m/z 66.0531 – see Scheme 2A, as well as losses of various low molecular weight structurally uninformative neutrals (e.g., NH_3, H_2O and -(NH_3+H_2O)), albeit with different ratios. However, several unique UVPD-MS/MS product ions were also observed. For example, the abundant ion at m/z 96.0634, assigned as $C_3H_7NO_2Li^+$, is proposed to be formed via a cis1,2 elimination reaction at the C3-C4 position of the alkyl chain (**Supplemental Scheme S1**). Notably, a pair of unique product ions were also observed at m/z 98.0790 and 122.0788 (losses of $C_{15}H_{28}$ and $C_{13}H_{28}$, respectively) (Δ 23.9998 Da). These ions were assigned as resulting from cis1,2 elimination at the C3-C4 and C5-C6 positions, respectively (i.e., either side of the sphingosine C4-C5 double bond), from the photoexcited

species resulting from absorption of 193 nm photons into the sphingosine double bond (**Scheme 2A**). These ions, analogous to those recently reported by Klein and Brodbelt [37] for assigning the location of double bonds within the acyl chains of protonated PC lipids, therefore provide confirmation of the position of the sphingosine double bond and allow this lipid to be readily distinguished from possible isomeric unsaturated dihydrosphingosine species (i.e., where the double bond would be located at other sites along the alkyl chain). Further evidence for this photo-absorption induced double bond selective fragmentation behaviour was obtained by examination of the spectra obtained from UVPD of the saturated sphingoid base, dihydrosphingosine d18:0 (Supplemental Figure S1A and **Scheme 2B**). In this spectrum, essentially no product ions were observed, presumably due to the low molar absorptivity of the saturated lipid [41,42].

UVPD- and HCD-MS/MS spectra acquired for the $[M+Li]^+$ precursor ion of sphingadiene d18:1(4E,11Z), containing C=C double bonds at both the C4 and C11 positions along the sphingoid base alkyl chain, are shown in **Figure 2A and 2B**, respectively. Similar to that described above for sphingosine, UVPD- yielded a pair of unique product ions differing by 24.0000 mass units (m/z 98.0790 and 122.0790), thereby confirming the presence of the sphingosine C4-C5 double bond (**Scheme 2C**). In addition, a second pair of product ions differing by 24.0000 mass units were also observed at m/z 194.1728 and 218.1728, corresponding to loss of C_8H_{14} and C_8H_{14} via cleavage of the C10-C11 and C12-C13 bonds, respectively, along the sphingoid chain. These ions therefore confirm the location of the C11-C12 unsaturated second double bond within the sphingadiene d18:1(4E,11Z) alkyl chain (Scheme 2C), similar to that reported by Klein and Brodbelt for unsaturated PC lipids [37], and demonstrates the ability of the UVPD technique to simultaneously localize multiple double bonds within a single alkyl chain.

Finally, similar information to that described above was also provided by UVPD- and HCD-MS/MS of the protonated (i.e., $[M+H]^+$) precursor ion of sphingadiene d18:1(4E,11Z) (Supplemental **Figure S2A and S2B**, respectively, and Supplemental **Scheme 2**). However, presumably due to the more limited 'mobility' of the Li adduct compared to a proton, we have observed that Li adduction generally promotes more effective charge remote fragmentation upon 193nm UVPD-MS/MS, resulting in the formation of more abundant double bond diagnostic product ions (e.g., compare the abundance of the sphingosine C4-C5 double bond diagnostic product ions at m/z 98.0791 and 122.0790 in Figure 2A with m/z 92.0711 and 116.0710 in Supplemental **Figure S2A)**.

<insert Figure 1 here>

<insert Figure 2 here>

<insert Scheme 2 here>

193 nm UVPD- and HCD-MS/MS of Ceramide Lipids

Ceramides consist of a fatty acyl chain of variable length linked via an amide bond to a sphingoid base (typically sphingosine or dihydrosphingosine). The amide-linked acyl chains are generally saturated or mono-unsaturated in mammalian cells, with chain lengths containing 16 to 24 carbons [43]. To further examine the 193nm UPVD induced formation of sphingosine C4-C5 double bond specific product ions in a more complex sphingolipid structure, UVPD-MS/MS was performed on the $[M+Li]^+$ precursor ion of ceramide d18:1(4E)/18:0, containing a sphingosine base and a saturated C18 amide-linked acyl chain, and is shown in **Figure 3A**. The corresponding HCD-MS/MS spectrum is shown in **Supplemental Figure S3A**. In both the UVPD- and HCD-MS/MS spectra, structurally diagnostic product ions are observed at m/z 245.2448 and 332.3129, corresponding to

cleavage of the sphingosine backbone (**Scheme 3A**), along with various structurally uninformative product ions formed via low molecular weight neutral losses. However, similar to that observed for the sphingosine and sphingadiene lipids in Figures 1A and 2A, a unique pair of diagnostic product ions at m/z 364.3391 and 388.3390 were observed in the UVPD spectrum, confirming the presence of the sphingosine C4-C5 double bond, while a second unique UVPD induced product ion at m/z 304.2818 (formed via cleavage of the amide bond, Scheme 3A) provided confirmation of the identity of the C18:0 saturated amide-linked acyl chain. UVPD- and HCD-MS/MS of the protonated (i.e., $[M+H]^+$) precursor ion of ceramide d18:0/18:1(9Z) (Supplemental **Figure S4A and S4B**, respectively, and Supplemental **Scheme 3**) was observed to fragment more efficiently compared to the lithiated adduct described above. However, the resultant UVPD fragmentation behavior was found to be more similar to those formed by collisional activation (i.e., HCD) [10], and the desired diagnostic fragments were generally found to be lower in relative abundance.

The UVPD-MS/MS spectrum for the $[M+Li]^+$ precursor ion of ceramide d18:0/18:1(9Z) containing a dihydrosphingosine base and an unsaturated fatty acid, i.e., a structural isomer of the ceramide d18:1(4E)/18:0 lipid in Figure 3A, is shown in **Figure 3B**. The corresponding HCD-MS/MS spectrum is shown in **Supplemental Figure S3B**. Analogous to the fragmentation behaviour described above for the sphingosine containing ceramide, UVPD- and HCD-MS/MS of the dihydrosphingosine containing ceramide d18:0/18:1(9Z) lipid resulted in the observation of characteristic product ions indicative of the dihydrosphingosine backbone (m/z 247.2606 and 330.2976, via cleavage at the C2-C3 position of the sphingoid base, **Scheme 3B**). The UVPD spectrum also contained a unique diagnostic amide bond cleavage product at m/z 306.2976, analogous to that observed in Figure 3A, confirming the presence of the mono-unsaturated C18:1 amide linked acyl chain. Notably, similar to the diagnostic ions described above for the sphingadiene C11-C12 double

bond in Figure 2A above, and reported by Klein and Brodbelt for unsaturated PC lipids [37], a unique pair of abundant product ions were also observed at m/z 434.4177 and 458.4177, corresponding to the loss of $C_{10}H_{18}$ and C_8H_{18} via cleavage of the C8-C9 and C10-C11 bonds along the fatty acyl chain, respectively. These ions therefore confirm the location of the C9-C10 unsaturated double bond within the C18:1 amide linked acyl chain (Scheme 3B).

Collectively, therefore, positive ionization mode 193nm UVPD-MS/MS of the $[M+Li]^+$ ions readily enables the differentiation and 'near-complete' structural characterization of these two structural isomeric species (note that the differentiation of cis/trans stereoisomers in both the C4 or C10 double bonds of these lipids is not possible using UVPD due to immediate photoisomerization of the double bond upon photon absorption, consistent with that previously described for the photochemistry of alkenes in solution – data not shown) [44].

<insert Figure 3 here>

<insert Scheme 3 here>

193 nm UVPD- and HCD-MS/MS of Complex Sphingolipids

Ceramide-1-phosphate

Having established the improved dissociation behaviour of 193 nm UVPD compared to HCD for simple sphingolipids, we next examined the effect of adding various head groups to ceramide (i.e., complex sphingolipid structures) on formation of the structurally diagnostic product ions described above. The simplest of the complex sphingolipids is ceramide-1-phosphate. Ceramide-1-phosphate is a bioactive sphingolipid synthesised intracellularly from direct phosphorylation of ceramide by ceramide kinase, and has been reported to be an

important mediator of cell growth, inflammatory response, anti-apoptotic signalling and cell migration [45]. As a representative example of this class of complex sphingolipid, UVPD- and HCD-MS/MS spectra were acquired for the $[M+2Li]^+$ adduct of ceramide-1-phosphate d18:1(4E)/16:0 (**Figure 4A and 4B**, respectively). Similar to that described above for the simple sphingolipids, in addition to the relatively structurally uninformative product ions observed by HCD involving dominant losses of the phosphate head group, UVPD also yielded an array of product ions that readily allowed confirmation of the sphingosine d18:1 backbone identity (m/z 390.2552) and the location of its C4-C5 double bond (m/z 422.2815 and 426.2812) (**Scheme 4**). For this lipid, the amide bond cleavage product ion corresponding to loss of the C16:0 saturated fatty acid chain (m/z 390.2567, $-C_{16}H_{32}O$) was isomeric with the C2-C3 sphingosine cleavage, so could not be independently confirmed.

<insert Figure 4 here>

<insert Scheme 4 here>

Sphingomyelin

Sphingomyelin, containing a phosphocholine head group attached to the 1-hydroxy group of a ceramide lipid, is the dominant class of sphingolipid enriched in the outer leaflet of plasma membranes within mammalian cells. In addition to being a major source of ceramides and other bioactive sphingolipids via the action of sphingomyelinases, sphingomyelins are also involved in various cellular functions including regulation of the activity of a number of membrane-bound proteins, and have been reported to be an independent risk factor in the development of cardiovascular disease [4,6]. To examine the fragmentation of this class of sphingolipid, UVPD- and HCD-MS/MS spectra were acquired for the $[M+Li]^+$ precursor ion of sphingomyelin d18:1(4E)/18:1(9Z) (**Scheme 5**), containing a

C18 sphingosine base and a mono-unsaturated C18:1 amide linked acyl chain (**Figure 5A** and **5B**, respectively). Similar to sphingosine (Figure 2A), the appearance of the diagnostic UVPD ion at m/z 495.3542, and the pair of ions at m/z 527.3804 and 551.3806 confirms the presence and identity of the sphingosine backbone, while the identity and structure of the C18:1 acyl chain is confirmed by the observation of the amide bond cleavage product ion at m/z 496.3386, and the pair of diagnostic double bond product ions at m/z 597.4593 and 621.4590 (Scheme 4). Thus, unlike HCD, 193nm UVPD can be employed for the detailed structural elucidation of complex sphingolipid structures in positive ionization mode, including those containing multiple sites of unsaturation in different alkyl chains.

<insert Figure 5 here>

<insert Scheme 5 here>

Glycosphingolipids

Glycosphingolipids are the most structurally diverse class of complex sphingolipids, containing one (e.g., glucosyl- and galactosyl-ceramides, and sulfatides) or more (e.g., lactosyl ceramides and gangliosides) sugar residues linked to ceramide via a β-glycosidic linkage [46,47]. Glycosphingolipids are involved in the mediation of biological functions as diverse as proliferation, differentiation, and apoptosis, and as specific membrane receptors of cellular recognition, adhesion, cell-cell communication, and membrane microdomain-mediated signal transduction [47-50].

As an example of the utility of 193nm UVPD for glycosphingolipid characterization, the product ion spectra acquired for the $[M+Li]^+$ adduct of galactosylceramide d18:1(4E)/24:1(15Z) is shown in **Figure 6A** (also see **Scheme 6A**). Despite the added head group complexity of this lipid, diagnostic sphingosine and fatty acyl C=C double bond

location specific products (i.e., m/z 632.4704 and 608.4704, and m/z 702.5487 and 678.5487, respectively) as well as sphingosine and amide bond specific cleavages (m/z 576.4440 and m/z 466.3346, respectively) were each observed. In addition, a series of galactose head group cleavage products were also observed, similar to those formed by HCD (**Figure 6B**) and CID (previously reported by Hsu and Turk [13]), thereby enabling the near complete structural characterization of this lipid. Although the 193 nm UVPD product ion spectrum of the glucosylceramide d18:1(4E)/24:1(15Z) epimer was found to be essentially identical to the galactosylceramide d18:1(4E)/24:1(15Z) lipid (data not shown), selective phenyl boronic acid complexation of the galactosylceramide *cis*1,2 diol moiety could potentially be used to differentiate between these epimers prior to UVPD, analogous to that described by Pham and Julian [22].

Finally, UVPD- and HCD-MS/MS spectra for the $[M+Li]^+$ adduct of another glycosphingolipid, lactosylceramide d18:1(4E)/24:0, were also acquired (see **Figure 7A and 7B**, respectively) (also see **Scheme 6B**). While the HCD spectrum was dominated by glycosidic cleavages similar to those previously reported for CID by Merrill *et al.* [12]. UVPD afforded dominant diagnostic products allowing unambiguous assignment of the sphingosine (m/z 740.5147) and amide-linked (m/z 628.3894) acyl chains, as well as a diagnostic pair of product ions enabling localization of the sphingosine C4-C5 double bond (m/z 796.5410 and 772.5406). Interestingly, while the majority of these cleavages were also reported by O'Brien *et al*. [36] for 193 nm UPVD of the singly deprotonated lactosylceramide d18:1/12:0, cleavages indicative of the sphingosine C=C double bond, or indicative of the sites of unsaturation within amide-linked acyl chains, were not reported in negative ionization mode.

<insert Figure 6 here>

<insert Figure 7 here>

<insert Scheme 6 here>

Finally, as an initial demonstration of the practical analytical utility of 193 nm UVPD-MS/MS for the characterization of endogenous lipids found within complex tissue extracts, two low or moderately abundant sphingolipid lipid species, namely hexosyl ceramide d18:1(4E/Z)/24:1(15Z/E) (Supplemental Figure S5A) and ceramide d18:1(4E/Z)/18:0 (Supplemental Figure S5B) were identified from their $[M+Li]^+$ precursor ions within a total lipid extract of porcine brain following its introduction to the mass spectrometer at a concentration of 50 μg/mL via nanoESI. Notably, the resultant spectra for these endogenous lipids, obtained with only 30 seconds of spectral averaging, were essentially identical to those obtained from the corresponding standards described above in Figures 6A and 3A, respectively). Furthermore, based on observation of the UVPD specific and structurally diagnostic sphingosine C=C and acyl chain C=C double bond cleavage product ions, and those formed by diagnostic cleavages of the N-C amide bond and sphingosine backbone, these spectra readily allowed the unambiguous differentiation of these lipid species from other potential isomeric lipids that could have been present. Note that as UVPD (or HCD)-MS/MS cannot differentiate between galactosyl and glucosyl ceramide headgroups, the endogenous lipid was assigned simply as a hexosyl ceramide. Also, as mentioned above, due to photoisomerization of cis/trans double bonds upon photon absorption, the locations of unsaturation within the endogenous lipids have been assigned ambiguously as E and/or Z (i.e., E/Z).

Conclusions

In this study, we have demonstrated the utility of 193 nm UVPD in positive ionization mode as an alternate ion activation method that enables the detailed structural characterization of a variety of different sphingolipid classes, including sphingoid bases, ceramides and complex sphingolipids. Importantly, UVPD was found to result in the formation of unique pairs of structurally diagnostic product ions indicative of the presence and site specific locations of both sphingosine and acyl chain C=C double bonds, as well as diagnostic ions enabling assignment of the sphingoid base and fatty acid identities, and head group structures. Although further studies are required in order to evaluate and extend this mode of ion activation to other lipid categories, as well as to explore the potential benefits of combining sequential HCD and UVPD, or other non-covalent adduction, to provide additional structural information such as sn-linkage positions within diacyl-containing lipid species, this approach clearly has great promise for improving the capabilities of tandem mass spectrometry methods for 'top down' shotgun lipidomics applications, and/or to reduce the burden of chromatographic fractionation methods that are commonly employed for the quantitative identification and quantification of complex lipid mixtures.

Acknowledgements

This work is dedicated to Scott McLuckey, to honor his receiving the 2016 ASMS Award for a Distinguished Contribution in Mass Spectrometry, and to gratefully acknowledge his thoughtful, patient and continuous support, as a mentor to G.E.R. and numerous other young scientists, throughout his career. We also thank Alexander Makarov and Andreas Kuehn for their assistance in enabling timing control of the laser pulses within the Orbitrap mass spectrometer software.

References

1. Fahy, E., Subramaniam, S., Murphy, R.C., Nishijima, M., Raetz, C.R.H., Shimizu, T., Spener, F., van Meer, G., Wakelam, M.J.O., Dennis, E.A.: Update of the LIPID MAPS comprehensive classification system for lipids. J. Lipid Res. **50**, S9–S14, (2009).
2. Breslow, D.K., Weissman, J.S.: Membranes in Balance: Mechanisms of Sphingolipid Homeostasis. Mol. Cell **40**, 267-279 (2010)
3. Hannun, Y.A., Obeid, L.M.: Principles of bioactive lipid signalling: lessons from sphingolipids. Nat. Rev. Mol. Cell Biol. **9**, 139-150 (2008).
4. Slotte, P.J.: Biological functions of sphingomyelins. Prog. Lipid Res. **52**, 424-437 (2013).
5. Maceyka, M., Spiegel, S.: Sphingolipid metabolites in inflammatory disease. Nature **510**, 58-67 (2014).
6. Slotte, P.J. Molecular properties of various structurally defined sphingomyelins -- correlation of structure with function. Prog Lipid Res. **52**, 206-219 (2013).
7. Ekroos, K. Lipidomics: Technologies & Applications; Wiley-VCH Verlag GmbH & Co.: Weinheim, Germany. (2012).
8. Merrill, Jr. A.H., Stokes, T.H., Momin, A., Park, H., Portz, B.J., Kelly, S., Wang, E., Sullards, C.M., Wang, M.D.: Sphingolipidomics: a valuable tool for understanding the roles of sphingolipids in biology and disease. J. Lipid Res. **50**, S97-S102 (2009).
9. Brügger B.: Lipidomics: analysis of the lipid composition of cells and subcellular organelles by electrospray ionization mass spectrometry. Annu. Rev. Biochem. 83, 79-98 (2014).
10. Murphy, R.C.: Tandem Mass Spectrometry of Lipids. Molecular Analysis of Complex Lipids. Royal Society of Chemistry, Cambridge, UK (2015)

11. Han, X.: Lipidomics: Comprehensive Mass Spectrometry of Lipids. John Wiley & Sons, Inc., Hoboken, New Jersey. (2016)

12. Merrill, Jr. A.H., Sullards, C.M., Allegood, J.C., Kelly, S., Wang, E.: Sphingolipidomics: High-throughput, structure-specific, and quantitative analysis of sphingolipids by liquid chromatography tandem mass spectrometry. Methods **36**, 207-224 (2005).

13. Hsu, F.F., Turk, J.: Structural determination of glycosphingolipids as lithiated adducts by electrospray ionization mass spectrometry using low-energy collisional-activated dissociation on a triple stage quadrupole instrument. J. Am. Soc. Mass Spectrom. **12**, 61-79 (2001).

14. Hsu, F.F., Turk, J.: Structural studies on ceramides as lithiated adducts by low energy collisional-activated dissociation tandem mass spectrometry with electrospray ionization. J. Am. Soc. Mass Spectrom. **13**, 680-695 (2002).

15. Hsu, F.F., Turk J.: Structural characterization of unsaturated glycerophospholipids by multiple-stage linear ion-trap mass spectrometry with electrospray ionization. J. Am. Soc. Mass Spectrom. 19, 1681-1691 (2008).

16. Hsu, F.F., Turk, J.: Electrospray ionization multiple-stage linear ion-trap mass spectrometry for structural elucidation of triacylglycerols: assignment of fatty acyl groups on the glycerol backbone and location of double bonds. J. Am. Soc. Mass Spec. **21**, 657-669 (2010).

17. Yang, K., Dilthey, B.G., Gross, R.W.: Identification and quantitation of fatty acid double bond positional isomers: a shotgun lipidomics approach using charge-switch derivatization Anal. Chem. **85**, 9742-9750 (2013).

18. Ma, X., Xia, Y.: Pinpointing double bonds in lipids by Paternò-Büchi reactions and mass spectrometry. Angew. Chem. Int. Ed. Engl. 53, 2592-2596 (2014).

19. Ma, X., Chong, L., Tian, R., Shi, R., Hu, T.Y., Ouyang, Z., Xia, Y.: Identification and quantitation of lipid C=C location isomers: A shotgun lipidomics approach enabled by photochemical reaction. Proc. Natl. Acad. Sci. U.S.A. **113**, 2573-2578 (2016).

20. Pham, H.T., Ly, T., Trevitt, A.J., Mitchell, T.W., Blanksby, S.: Differentiation of complex lipid isomers by radical-directed dissociation mass spectrometry. Anal. Chem. **84**, 7525-7532 (2012).

21. Pham, H.T., Julian, R.R.: Radical delivery and fragmentation for structural analysis of glycerophospholipids. Int. J. Mass Spectrom. **370**, 58-65 (2014).

22. Pham, H.T., Julian, R.R.: Characterization of glycosphingolipid epimers by radical-directed dissociation mass spectrometry. Analyst **141**, 1273-1278 (2016).

23. Thomas, M.C., Mitchell, T.W., Harman, D.G., Deeley, J.M., Nealon, J.R., Blanksby, S.J. Ozone-induced dissociation: elucidation of double bond position within mass-selected lipid ions. Anal. Chem. **80**, 303-311 (2008).

24. Brown, S.H., Mitchell, T.W., Blanksby, S.J.: Analysis of unsaturated lipids by ozone-induced dissociation. Biochim Biophys Acta. **1811**, 807-817 (2011).

25. Pham, H.T., Maccarone, A.T., Thomas, M.C., Campbell, J.L., Mitchell, T.W., Blanksby, S.J.: Structural characterization of glycerophospholipids by combinations of ozone- and collision-induced dissociation mass spectrometry: the next step towards "top-down" lipidomics. Analyst. **139**, 204-214 (2014).

26. Jones, J.W., Thompson, C.J., Carter, C.L., Kane, M.A.: Electron-induced dissociation (EID) for structure characterization of glycerophosphatidylcholine: determination of double-bond positions and localization of acyl chains. J. Mass Spectrom. **50**, 1327-1339 (2015).

27. Campbell, J.L., Baba, T.: Near-complete structural characterization of phosphatidylcholines using electron impact excitation of ions from organics. Anal. Chem. **87**, 5837-5845 (2015).

28. Baba, T., Campbell, J.L., Yves Le Blanc, J.C., Baker, P.R.S.: In-depth sphingomyelin characterization using electron impact excitation of ions from organics and mass spectrometry. J. Lipid Res. **57**, 858-867 (2016).

29. Deimler, R.E., Sander, M., Jackson, G.P.: Radical-induced fragmentation of phospholipid cations using metastable atom-activated dissociation mass spectrometry (MAD-MS). Int. J. Mass Spectrom. **290**, 178-186 (2015).

30. Brodbelt, J.S.: Photodissociation mass spectrometry: new tools for characterization of biological molecules. Chem. Soc. Rev. **43**, 2757-2783 (2014).

31. Devakumar, A., O'Dell, D.K., Walker, J.M., Reilly, J.P.: Structural analysis of leukotriene C4 isomers using collisional activation and 157 nm photodissociation. J. Am. Soc. Mass Spectrom. **19**, 14-26 (2008).

32. Madsen, J.A., Cullen, T.W., Trent, M.S., Brodbelt, J.S.: IR and UV photodissociation as analytical tools for characterizing lipid A structures. Anal Chem. **83**, 5107-5113 (2011).

33. O'Brien, J.P., Needham, B.D., Henderson, J.C., Nowicki, E.M., Trent, M.S., Brodbelt, J.S.: 193 nm Ultraviolet photodissociation mass spectrometry for the structural elucidation of lipid A compounds in complex mixtures. Anal. Chem. **86**, 2138-2145 (2014).

34. Boll, J.M., Tucker, A.T., Klein, D.R., Beltran, A.M., Brodbelt, J.S., Davies, B.W., Trent, M.S.: Reinforcing Lipid A Acylation on the Cell Surface of *Acinetobacter baumannii* Promotes Cationic Antimicrobial Peptide Resistance and Desiccation Survival. mBio. **6**, e00478-15 (**2015**).

35. Klein, D.R., Holden, D.D., Brodbelt, J.S.: Shotgun Analysis of Rough-Type Lipopolysaccharides Using Ultraviolet Photodissociation Mass Spectrometry. Anal Chem. **88**, 1044-1051 (2016).

36. O'Brien, J.P., Brodbelt, J.S.: Structural characterization of gangliosides and glycolipids via ultraviolet photodissociation mass spectrometry. Anal. Chem. **85**, 10399-10407 (2013).

37. Klein, D.R., Brodbelt, J.S.: Structural Characterization of Phosphatidylcholines Using 193 nm Ultraviolet Photodissociation Mass Spectrometry. Anal Chem. **89**, 1516-1522 (2017).

38. Fort, K.L., Dyachenko, A., Potel, C.M., Corradini, E., Marino, F., Barendregt, A., Makarov, A.A., Scheltema, R.A., Heck, A.J.R.: Implementation of ultraviolet photodissociation on a benchtop Q exactive mass spectrometer and its application to phosphoproteomics. Anal. Chem. **88**, 2303-2310 (2016).

39. Merrill Jr., A.H., Sandhoff, K.: New comprehensive biochemistry: Biochemistry of lipids, lipoproteins, and membranes, (Chapter 14) D.E. Vance, J.E. Vance (Eds.), Elsevier, Amsterdam (2002).

40. Pruett, S.T., Bushnev, A., Hagedorn, K., Adiga, M., Haynes, C.A., Sullards, M.C., Liotta, D.C. and Merrill, A.H.: Biodiversity of sphingoid bases ('sphingosines') and related amino alcohols. *J. Lipid Res.*, **49**, 1621-1639 (2008).

41. Barnes, R.H., Rusoff, I.I., Miller, E.S., Burr, G.O.: Relationship between Unsaturation and Ultraviolet Absorption Spectra of Various Fats and Fatty Acids. Ind. Eng. Chem. Anal. Ed., **16**, 385–386 (1944).

42. Rusoff, I.I., Platt, J.R., Klevens, H.B., Burr, G.O.: Extreme Ultraviolet Absorption Spectra of the Fatty Acids. J. Am. Soc. Chem. **67**, 673-678 (1945).

43. Castro, B.M., Prieto, M., Silva, L.C.: Ceramide: a simple sphingolipid with unique biophysical properties. Prog Lipid Res. **54**, 53-67 (2014)

44. Kropp, P.J.: Photochemistry of alkenes in solution. Pure Appl. Chem. **24**, 585-598 (1970).

45. Presa, N., Gomez-Larrauri, A., Rivera, I.G., Ordoñez, M., Trueba, M., Gomez-Muñoz, A.: Regulation of cell migration and inflammation by ceramide 1-phosphate. Biochim. Biophys. Acta. **1861**, 402-409 (2016).

46. Schnaar, R.L., Suzuki, A., Stanley, P.: Glycosphingolipids. In: Essentials of Glycobiology. 2nd Ed. Varki, Cummings, Esko, Freeze, Stanley, Bertozzi, Hart and Etzler., editors. Cold Spring Harbor (NY): Cold Spring Harbor Laboratory Press. Chpt. 10, (2009).

47. Yu, R.K., Tsai, Y.T., Ariga, T., Yanagisawa, M.: Structures, biosynthesis, and functions of gangliosides--an overview. J. Oleo. Sci. **60**, 537-544 (2011).

48. Lingwood, C.A.: Glycosphingolipid Functions. Cold Spring Harb. Perspect. Biol. **3**, a004788 (2011).

49. Iwabuchi, K., Nakayama, H., Iwahara, C., Takamori, K.: Significance of glycosphingolipid fatty acid chain length on membrane microdomain-mediated signal transduction. FEBS Lett. **584**, 1642-1652 (2010).

50. d'Azzo, A., Tessitore, A., Sano, R.: Gangliosides as apoptotic signals in ER stress response. Cell Death Differ. **13**, 404-414 (2006).

Figure Legends

Figure 1. (A) 193 nm UVPD- and (B) HCD-MS/MS of the $[M+Li]^+$ precursor ion of sphingosine d18:1. Structurally diagnostic UVPD specific product ions corresponding to cleavage of the sphingosine C=C double bond are indicated using red text. Structurally diagnostic sphingosine backbone cleavage product ions common to both HCD and UVPD are indicated in blue text. See Scheme 2a and B for structural information.

Figure 2. (A) 193nm UVPD- and (B) HCD-MS/MS of the $[M+Li]^+$ precursor ion of sphingadiene d18:2(4E,11Z). Structurally diagnostic UVPD specific product ions corresponding to cleavage of the sphingosine C=C and alkyl chain C=C double bonds (panel A) are indicated using red text. Structurally diagnostic sphingosine backbone product ions common to both HCD and UVPD are indicated in blue text. See Scheme 2C for structural information.

Figure 3. 193 nm UVPD-MS/MS of the $[M+Li]^+$ precursor ions of the isomeric lipid species (A) ceramide d18:1(4E)/18:0 and (B) dihydroceramide d18:0/18:1(9Z). Structurally diagnostic UVPD specific product ions corresponding to cleavage of the sphingosine C=C (panel A) or acyl chain C=C (panel B) double bonds are indicated using red text, while those corresponding to cleavage of the N-C amide bond are indicated using green text (panels A and B). Structurally diagnostic sphingosine backbone product ions common to both HCD and UVPD are indicated in blue text. See Scheme 3 for structural information.

Figure 4. (A) 193 nm UVPD- and (B) HCD-MS/MS of the $[M-H+2Li]^+$ precursor ion of ceramide 1-phosphate d18:1(4E)/16:0. Structurally diagnostic UVPD specific product ions corresponding to cleavage of the sphingosine C=C double bond are indicated using red text, while those corresponding to cleavage of the N-C amide bond or sphingosine backbone are indicated using green and blue text, respectively. See Scheme 4 for structural information.

Figure 5. (A) 193 nm UVPD- and (B) HCD-MS/MS of the $[M+Li]^+$ precursor ion of sphingomyelin d18:1(4E)/18:1(9Z). Structurally diagnostic UVPD specific product ions corresponding to cleavage of the sphingosine C=C and acyl chain C=C double bonds are indicated using red text, while those corresponding to cleavage of the N-C amide bond and sphingosine backbone are indicated using green and blue text, respectively. See Scheme 5 for structural information.

Figure 6. (A) 193 nm UVPD- and (B) HCD-MS/MS of the $[M+Li]^+$ precursor ion of galactosyl ceramide d18:1(4E)/24:1(15Z). Structurally diagnostic UVPD specific product ions corresponding to cleavage of the sphingosine C=C and acyl chain C=C double bonds are indicated using red text, while those corresponding to cleavage of the N-C amide bond and sphingosine backbone are indicated using green and blue text, respectively. See Scheme 6A for structural information.

Figure 7. (A) 193 nm UVPD- and (B) HCD-MS/MS of the $[M+Li]^+$ precursor ion of lactosyl ceramide d18:1(4E)/24:0. Structurally diagnostic UVPD specific product ions corresponding to cleavage of the sphingosine C=C double bond are indicated using red text, while those corresponding to cleavage of the N-C amide bond and

sphingosine backbone are indicated using green and blue text, respectively. See Scheme 6B for structural information.

Legends to Schemes

Scheme 1. Overview of the major lipid classes involved in sphingolipid metabolism. Representative lipid species from sphingolipid classes or subclasses labelled in bold text were examined in this study.

Scheme 2. Summary of the 193 nm UVPD-MS/MS dissociation behaviour of the $[M+Li]^+$ precursor ions of (A) sphingosine d18:1(4E), (B) dihydrosphingosine d18:0 and (C) sphingadiene d18:2(4E,11Z). Structurally diagnostic UVPD specific product ions corresponding to cleavage of the sphingosine C=C (panels A and C) and acyl chain C=C (panel C) double bonds are indicated using red text, while structurally diagnostic sphingosine backbone cleavage product ions common to both HCD and UVPD are indicated in blue text. Arrows show the proposed mechanisms for formation of the sphingosine C=C and alkyl chain C=C double bond specific product ions.

Scheme 3. Summary of the 193 nm UVPD-MS/MS dissociation behaviour of the $[M+Li]^+$ precursor ions of the isomeric lipid species (A) ceramide d18:1(4E)/18:0 and (B) dihydroceramide d18:0/18:1(9Z). Structurally diagnostic UVPD specific product ions corresponding to cleavage of the sphingosine C=C (panel A) or acyl chain C=C (panel B) double bonds are indicated using red text, while those corresponding to cleavage of the N-C amide bond are indicated using green text

(panels A and B). Structurally diagnostic sphingosine backbone cleavage product ions common to both HCD and UVPD are indicated in blue text.

Scheme 4. Summary of the 193 nm UVPD-MS/MS dissociation behaviour of the $[M+2Li]^+$ precursor ion of ceramide 1-phosphate d18:1(4E)/16:0. Structurally diagnostic UVPD specific product ions corresponding to cleavage of the sphingosine C=C double bond are indicated using red text, while those corresponding to cleavage of the N-C amide bond or sphingosine backbone are indicated using green and blue text, respectively.

Scheme 5. Summary of the 193 nm UVPD-MS/MS dissociation behaviour of the $[M+Li]^+$ precursor ions of sphingomyelin d18:1(4E)/18:1(9Z). Structurally diagnostic UVPD specific product ions corresponding to cleavage of the sphingosine C=C and acyl chain C=C double bonds are indicated using red text, while those corresponding to cleavage of the N-C amide bond and sphingosine backbone are indicated using green and blue text, respectively.

Scheme 6. Summary of the 193 nm UVPD-MS/MS dissociation behaviour of the $[M+Li]^+$ precursor ion of (A) galactosyl ceramide d18:1(4E)/24:1(15Z) and (B) lactosyl ceramide d18:1(4E)/24:0. Structurally diagnostic UVPD specific product ions corresponding to cleavage of the acyl chain C=C and/or sphingosine C=C double bonds are indicated using red text, while those corresponding to cleavage of the N-C amide bond and sphingosine backbone are indicated using green and blue text, respectively.

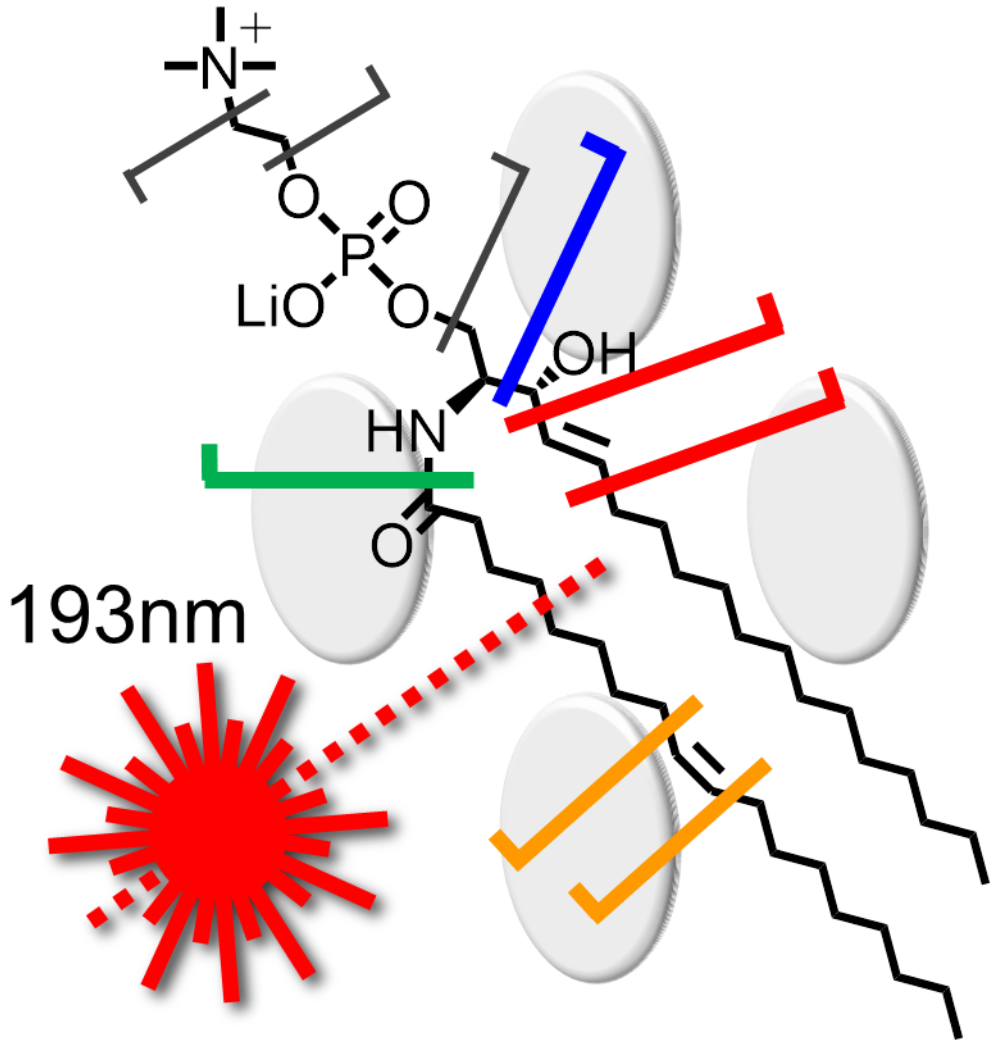
N+
O
O
P
O
LiO
O
OH
HN
O
193nm

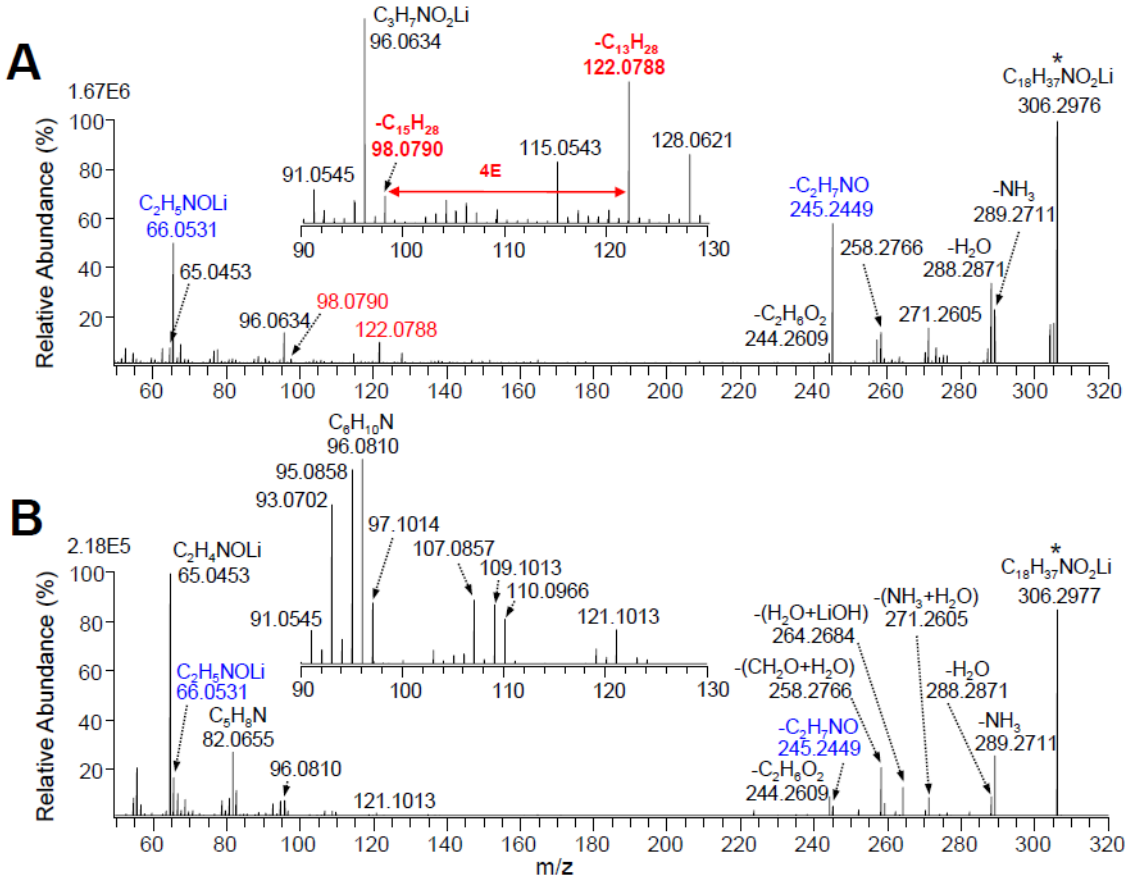
A
1.67E6
Relative Abundance (%)
C3H7NO2Li
96.0634
-C13H28
122.0788
-C15H28
98.0790
4E
115.0543
128.0621
91.0545
C2H5NOLi
66.0531
65.0453
96.0634
98.0790
122.0788
-C2H7NO
245.2449
258.2766
-H2O
288.2871
-NH3
289.2711
-C2H6O2
244.2609
271.2605
*
C18H37NO2Li
306.2976
B
2.18E5
C6H10N
96.0810
95.0858
93.0702
97.1014
107.0857
109.1013
110.0966
121.1013
91.0545
C2H4NOLi
65.0453
C2H5NOLi
66.0531
C5H8N
82.0655
96.0810
121.1013
-(H2O+LiOH)
264.2684
-(NH3+H2O)
271.2605
-(CH2O+H2O)
258.2766
-H2O
288.2871
-NH3
289.2711
-C2H7NO
245.2449
-C2H6O2
244.2609
*
C18H37NO2Li
306.2977
m/z

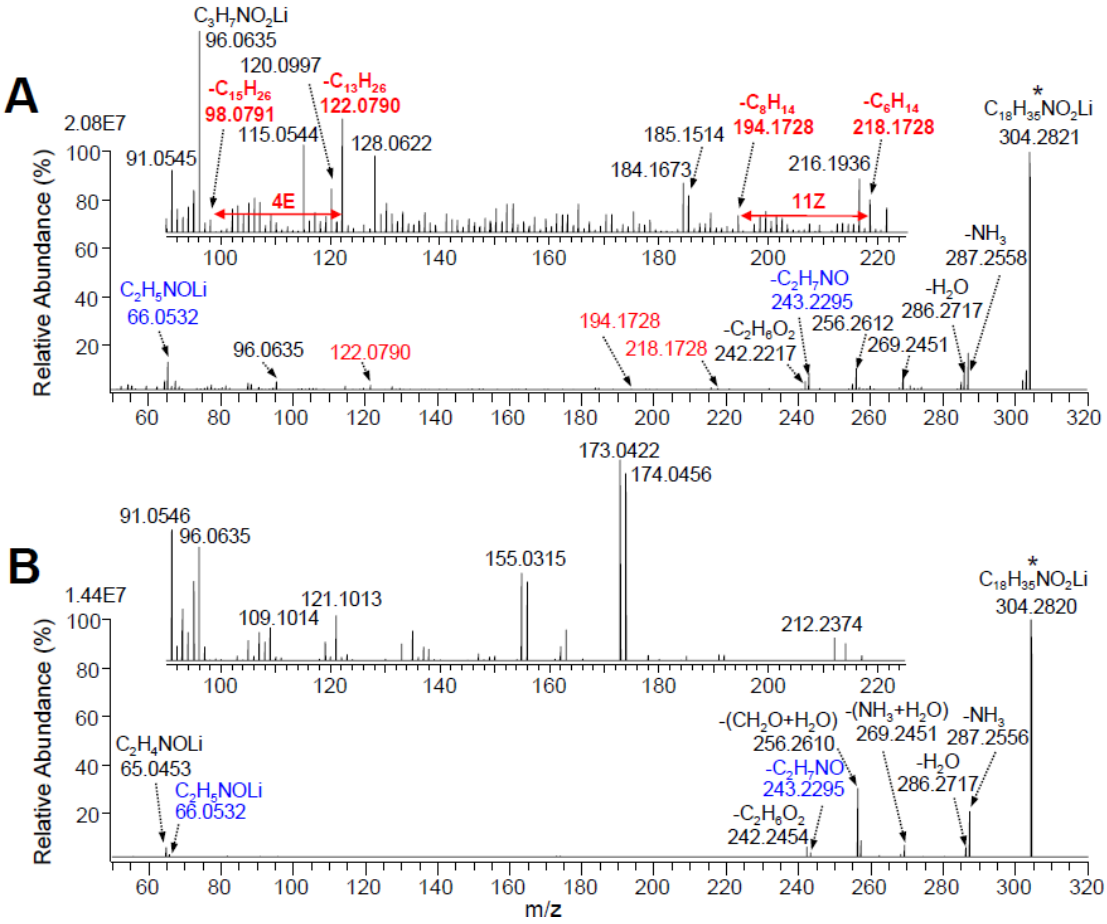
A
2.08E7
Relative Abundance (%)
C3H7NO2Li
96.0635
120.0997
-C15H26
98.0791
-C13H26
122.0790
115.0544
128.0622
91.0545
4E
185.1514
-C8H14
194.1728
-C6H14
218.1728
184.1673
216.1936
11Z
*
C18H35NO2Li
304.2821
-NH3
287.2558
-H2O
286.2717
C2H5NOLi
66.0532
-C2H7NO
243.2295
256.2612
269.2451
-C2H6O2
242.2217
194.1728
218.1728
96.0635
122.0790
B
1.44E7
173.0422
174.0456
91.0546
96.0635
155.0315
121.1013
109.1014
212.2374
*
C18H35NO2Li
304.2820
C2H4NOLi
65.0453
C2H5NOLi
66.0532
-(CH2O+H2O)
256.2610
-(NH3+H2O)
269.2451
-NH3
287.2556
-H2O
286.2717
-C2H7NO
243.2295
-C2H6O2
242.2454
m/z

Figure 3

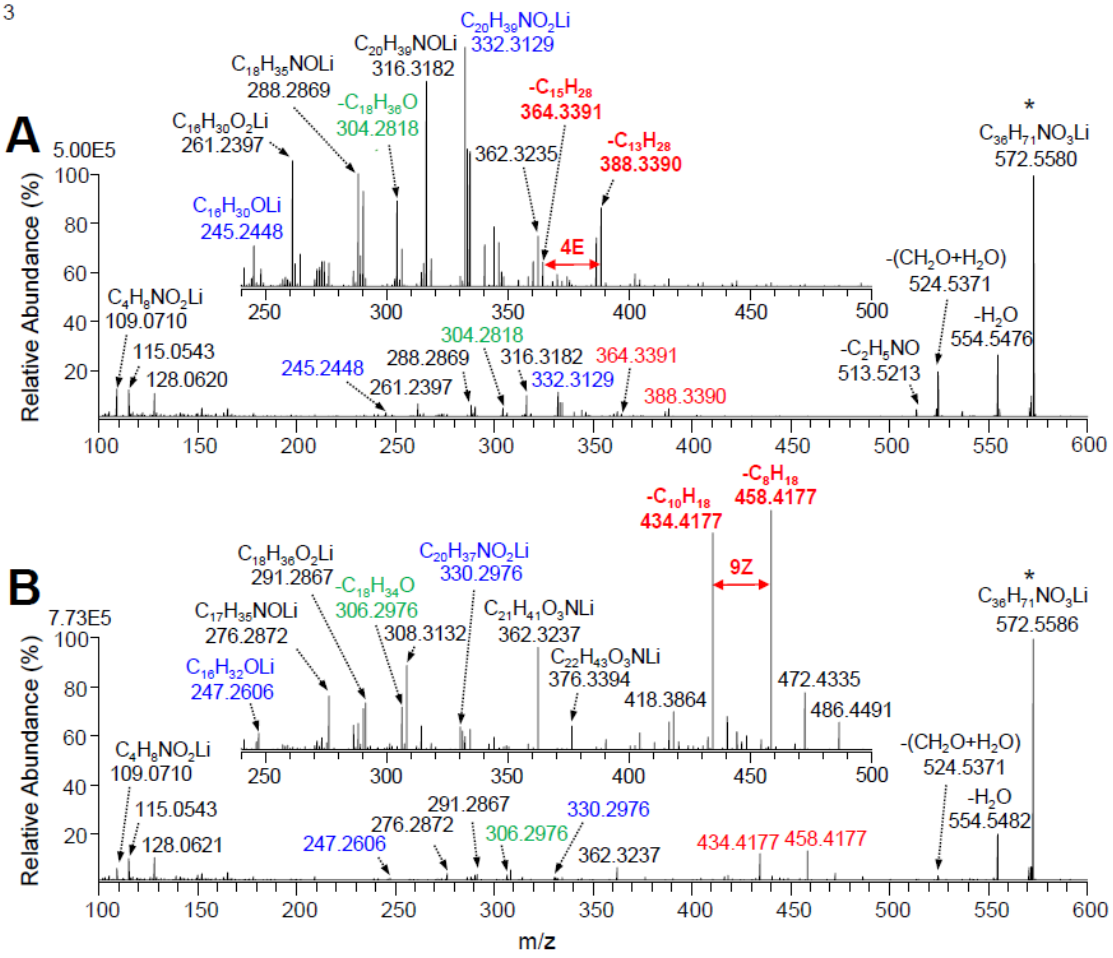
A
5.00E5
Relative Abundance (%)
C20H39NO2Li 332.3129
C20H36NOLi 316.3182
C18H35NOLi 288.2869
-C18H36O 304.2818
C16H30O2Li 261.2397
-C15H28 364.3391
-C13H28 388.3390
362.3235
C16H30OLi 245.2448
4E
*
C36H71NO3Li 572.5580
-(CH2O+H2O) 524.5371
-H2O 554.5476
-C2H5NO 513.5213
C4H8NO2Li 109.0710
115.0543
128.0620
304.2818
288.2869
316.3182
364.3391
245.2448
261.2397
332.3129
388.3390
B
7.73E5
-C10H18 434.4177
-C8H18 458.4177
9Z
C18H36O2Li 291.2867
-C18H34O 306.2976
C20H37NO2Li 330.2976
C17H35NOLi 276.2872
308.3132
C21H41O3NLi 362.3237
C16H32OLi 247.2606
C22H43O3NLi 376.3394
418.3864
472.4335
486.4491
*
C36H71NO3Li 572.5586
-(CH2O+H2O) 524.5371
-H2O 554.5482
C4H8NO2Li 109.0710
115.0543
128.0621
291.2867
276.2872
330.2976
306.2976
247.2606
362.3237
434.4177
458.4177
m/z

Figure 4

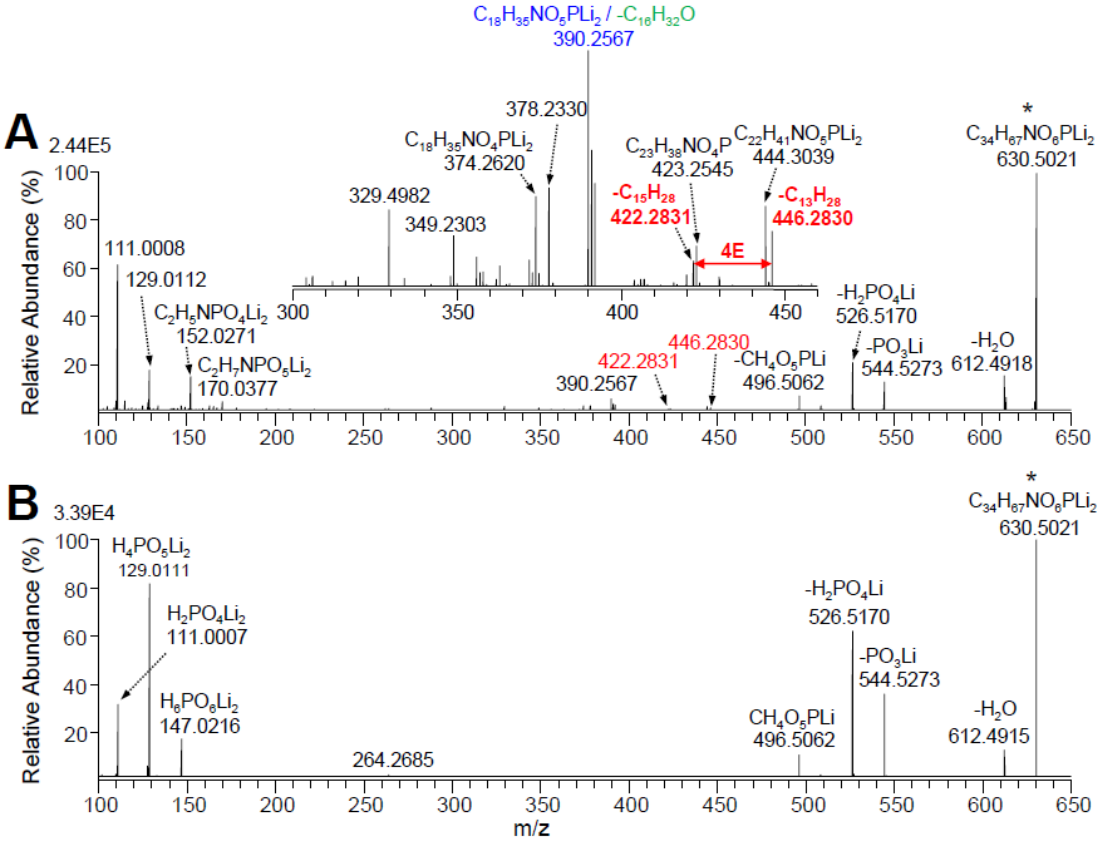
A
2.44E5
Relative Abundance (%)
$C_{18}H_{35}NO_5PLi_2$ / $-C_{16}H_{32}O$
390.2567
378.2330
$C_{18}H_{35}NO_4PLi_2$
374.2620
$C_{23}H_{38}NO_4P$
423.2545
$C_{22}H_{41}NO_5PLi_2$
444.3039
$C_{34}H_{67}NO_6PLi_2$
630.5021
329.4982
349.2303
$-C_{15}H_{28}$
422.2831
$-C_{13}H_{28}$
446.2830
4E
111.0008
129.0112
$C_2H_5NPO_4Li_2$
152.0271
$C_2H_7NPO_5Li_2$
170.0377
$-H_2PO_4Li$
526.5170
$-PO_3Li$
544.5273
$-H_2O$
612.4918
446.2830
422.2831
390.2567
$-CH_4O_5PLi$
496.5062
B
3.39E4
$H_4PO_5Li_2$
129.0111
$H_2PO_4Li_2$
111.0007
$H_6PO_6Li_2$
147.0216
264.2685
CH_4O_5PLi
496.5062
$-H_2PO_4Li$
526.5170
$-PO_3Li$
544.5273
$-H_2O$
612.4915
$C_{34}H_{67}NO_6PLi_2$
630.5021
m/z

Figure 5

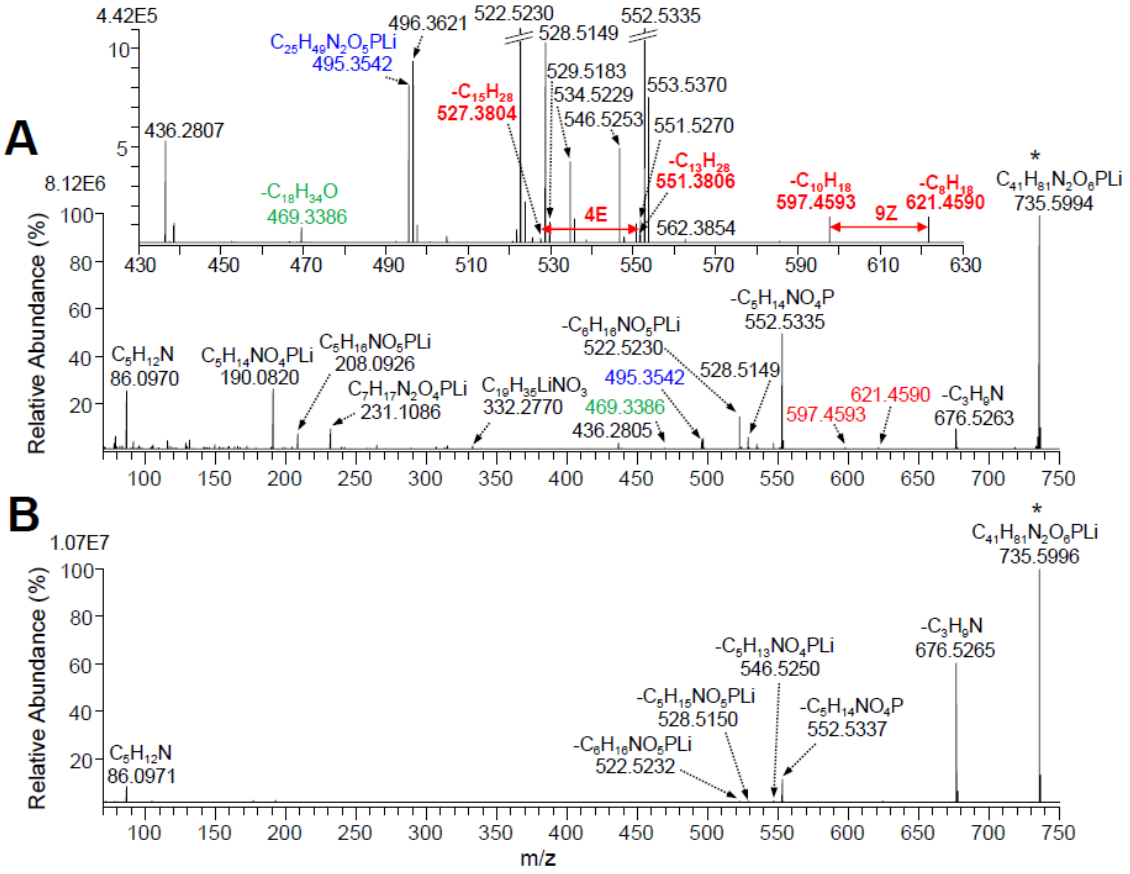
A
4.42E5
8.12E6
Relative Abundance (%)
C25H49N2O5PLi
495.3542
496.3621
522.5230
528.5149
552.5335
529.5183
534.5229
553.5370
546.5253
551.5270
562.3854
436.2807
-C18H34O
469.3386
-C15H28
527.3804
-C13H28
551.3806
4E
-C10H18
597.4593
9Z
-C8H18
621.4590
*
C41H81N2O6PLi
735.5994
-C5H14NO4P
552.5335
-C6H16NO5PLi
522.5230
C5H12N
86.0970
C5H14NO4PLi
190.0820
C5H16NO5PLi
208.0926
C7H17N2O4PLi
231.1086
C19H35LiNO3
332.2770
495.3542
469.3386
436.2805
528.5149
621.4590
597.4593
-C3H9N
676.5263
B
1.07E7
Relative Abundance (%)
*
C41H81N2O6PLi
735.5996
-C3H9N
676.5265
-C5H13NO4PLi
546.5250
-C5H15NO5PLi
528.5150
-C5H14NO4P
552.5337
-C6H16NO5PLi
522.5232
C5H12N
86.0971
m/z

Figure 6

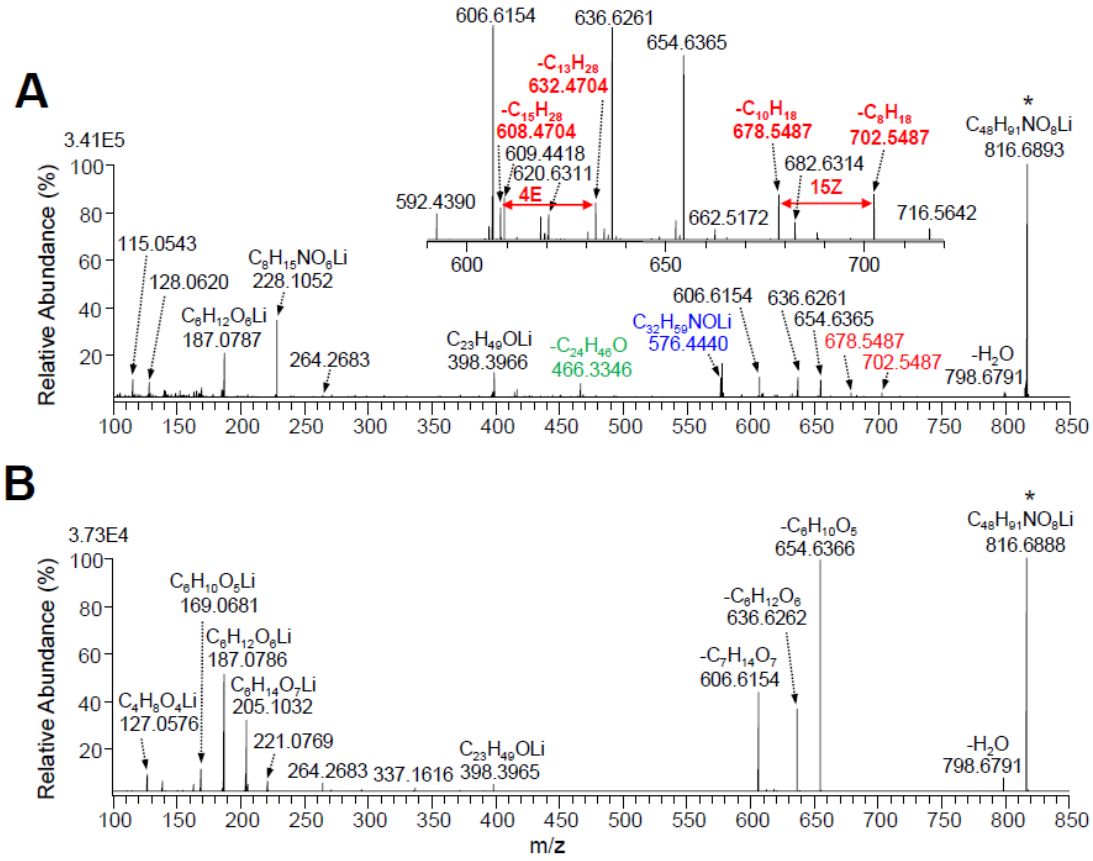
A
3.41E5
Relative Abundance (%)
606.6154
636.6261
654.6365
-C13H28
632.4704
-C15H28
608.4704
609.4418
620.6311
4E
592.4390
662.5172
-C10H18
678.5487
-C8H18
702.5487
682.6314
15Z
716.5642
*
C48H91NO8Li
816.6893
115.0543
128.0620
C8H15NO6Li
228.1052
C6H12O6Li
187.0787
264.2683
C23H49OLi
398.3966
-C24H46O
466.3346
C32H59NOLi
576.4440
606.6154
636.6261
654.6365
678.5487
702.5487
-H2O
798.6791
B
3.73E4
Relative Abundance (%)
-C6H10O5
654.6366
*
C48H91NO8Li
816.6888
C6H10O5Li
169.0681
C6H12O6Li
187.0786
C6H14O7Li
205.1032
C4H8O4Li
127.0576
221.0769
264.2683
337.1616
C23H49OLi
398.3965
-C6H12O6
636.6262
-C7H14O7
606.6154
-H2O
798.6791
m/z

Figure 7

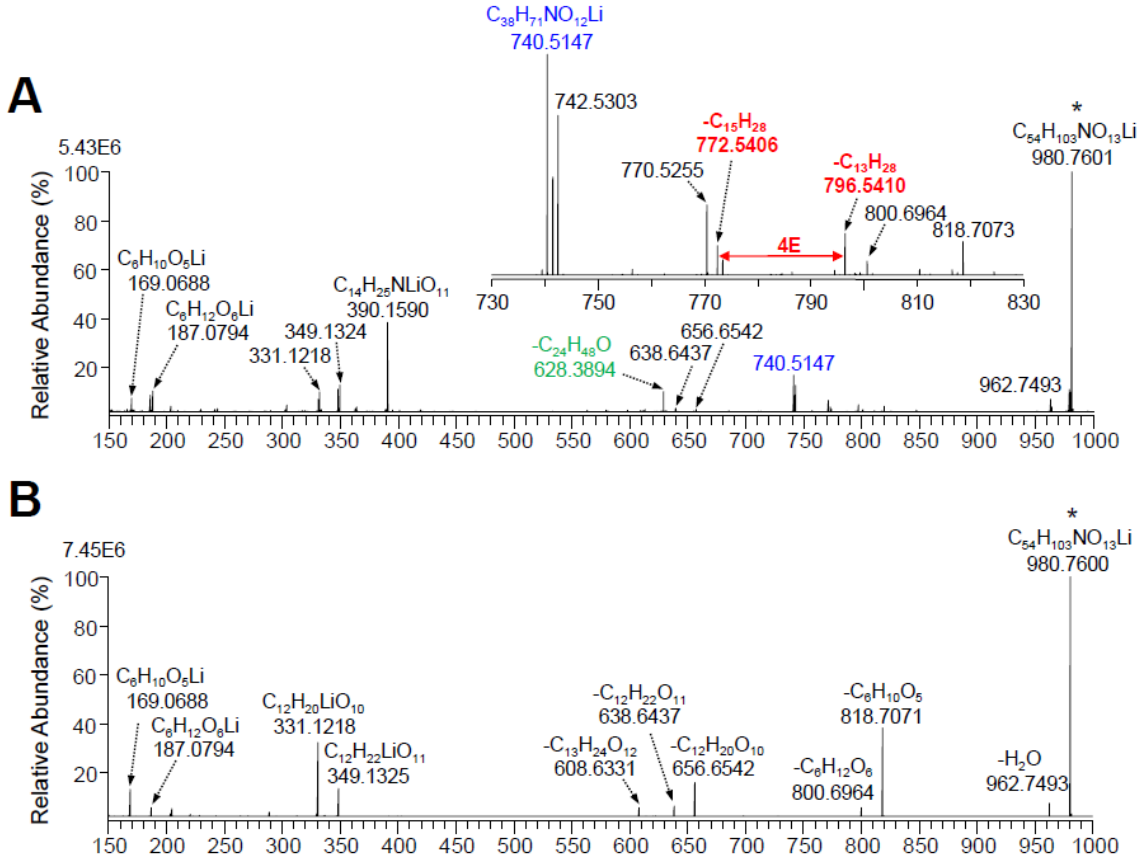
A
5.43E6
Relative Abundance (%)
C38H71NO12Li
740.5147
742.5303
-C15H28
772.5406
770.5255
-C13H28
796.5410
800.6964
818.7073
4E
*
C54H103NO13Li
980.7601
C6H10O5Li
169.0688
C6H12O6Li
187.0794
C14H25NLiO11
390.1590
349.1324
331.1218
-C24H48O
628.3894
656.6542
638.6437
740.5147
962.7493
B
7.45E6
Relative Abundance (%)
*
C54H103NO13Li
980.7600
C6H10O5Li
169.0688
C6H12O6Li
187.0794
C12H20LiO10
331.1218
C12H22LiO11
349.1325
-C12H22O11
638.6437
-C13H24O12
608.6331
-C12H20O10
656.6542
-C6H10O5
818.7071
-C6H12O6
800.6964
-H2O
962.7493

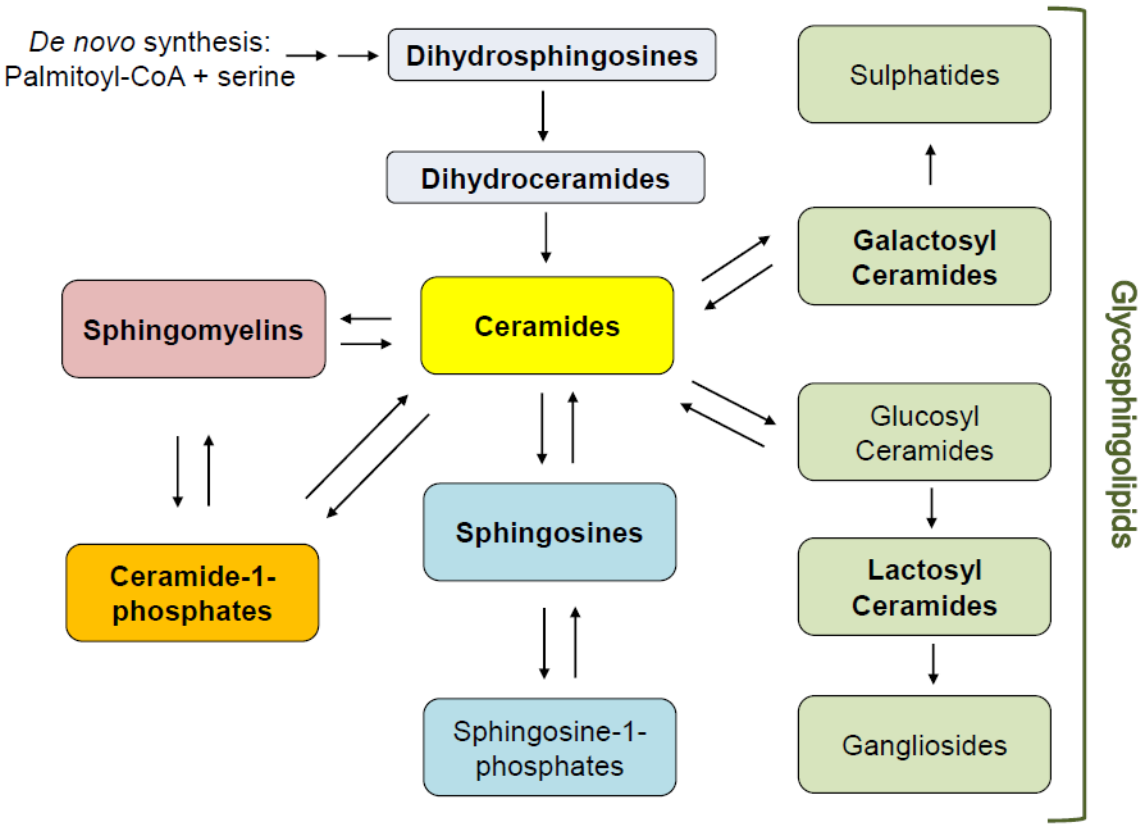
De novo synthesis:
Palmitoyl-CoA + serine
Dihydrosphingosines
Dihydroceramides
Sphingomyelins
Ceramides
Ceramide-1-phosphates
Sphingosines
Sphingosine-1-phosphates
Sulphatides
Galactosyl Ceramides
Glucosyl Ceramides
Lactosyl Ceramides
Gangliosides
Glycosphingolipids

Scheme 2

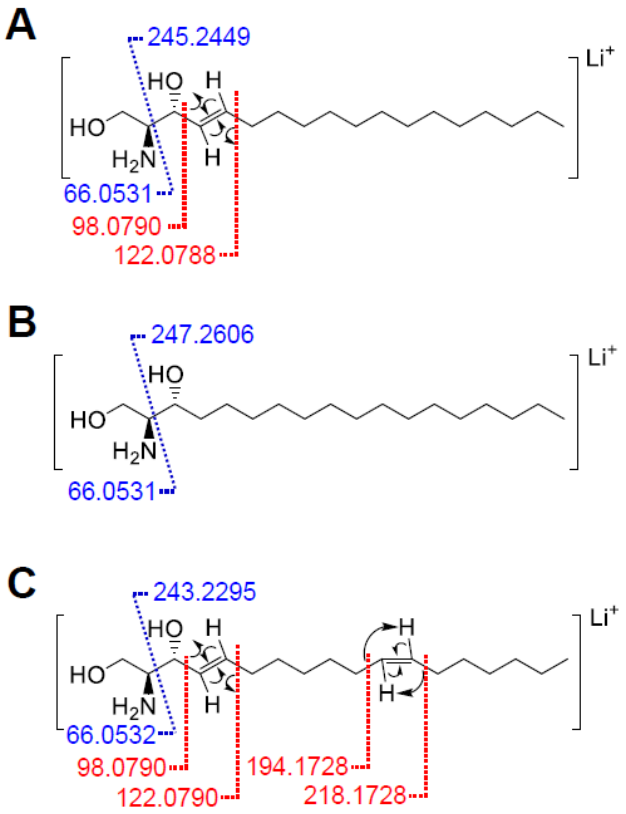
A
245.2449
HO
H
HO
H2N
H
Li+
66.0531
98.0790
122.0788
B
247.2606
HO
HO
H2N
Li+
66.0531
C
243.2295
HO
H
HO
H2N
H
H
H
Li+
66.0532
98.0790
122.0790
194.1728
218.1728

Scheme 3

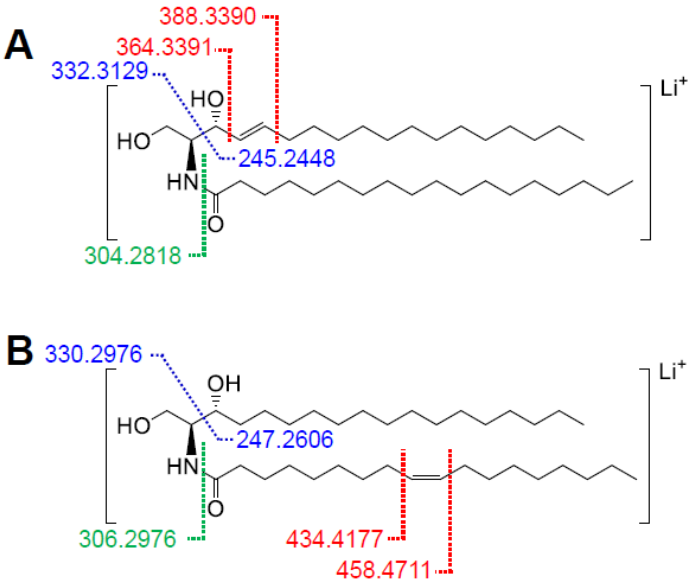
A
388.3390
364.3391
332.3129
HO
HO
HN
O
245.2448
304.2818
Li+
B
330.2976
OH
HO
HN
O
247.2606
306.2976
434.4177
458.4711
Li+

Scheme 4

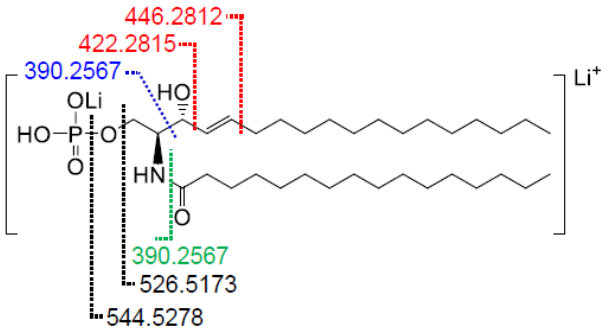
446.2812
422.2815
390.2567
OLi
HO
HO
P
O
O
HN
O
Li+
390.2567
526.5173
544.5278

Scheme 5

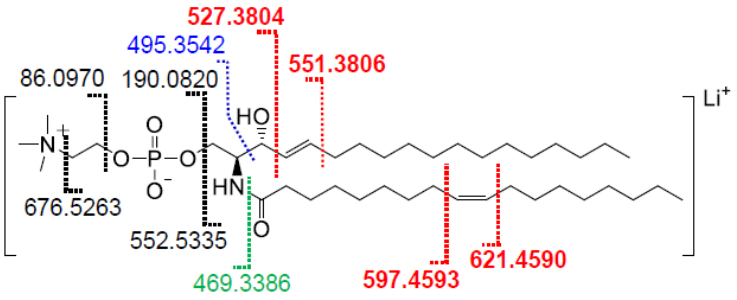
527.3804
495.3542
551.3806
86.0970
190.0820
Li+
HO
HN
676.5263
552.5335
469.3386
597.4593
621.4590

Scheme 6

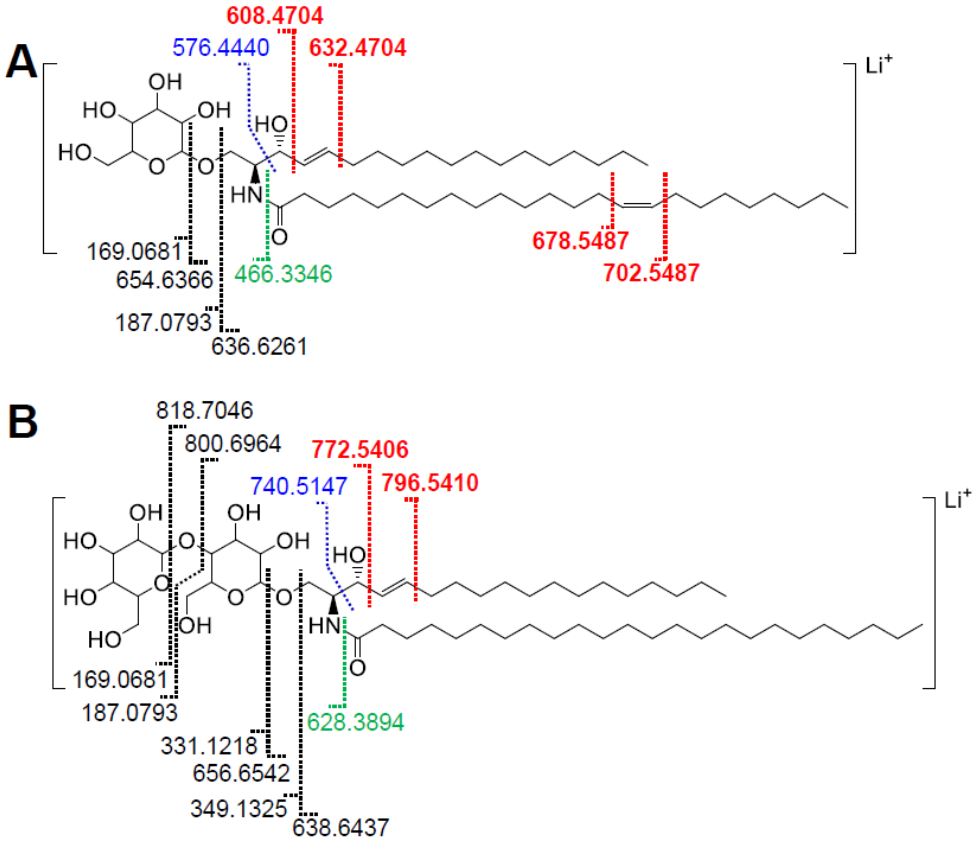
A
608.4704
576.4440
632.4704
Li+
OH
HO
OH
HO
HO
O
O
HN
O
169.0681
654.6366
466.3346
187.0793
636.6261
678.5487
702.5487
B
818.7046
800.6964
772.5406
740.5147
796.5410
Li+
OH
OH
HO
O
OH
HO
HO
O
O
O
OH
HO
HN
O
169.0681
187.0793
628.3894
331.1218
656.6542
349.1325
638.6437

Supplemental Information

Detailed Structural Characterization of Sphingolipids via 193 nm Ultraviolet Photodissociation and Ultra High Resolution Tandem Mass Spectrometry

Eileen Ryan[1], Catherine Quynh Nguyen[1], Christopher Shiea[1] and Gavin E. Reid[1,2,3*]

[1]School of Chemistry, [2]Department of Biochemistry and Molecular Biology, [3]Bio21 Molecular Science and Biotechnology Institute. University of Melbourne, Parkville, Victoria 3010, Australia

*Address Correspondence to: gavin.reid@unimelb.edu.au

Supplemental Figures

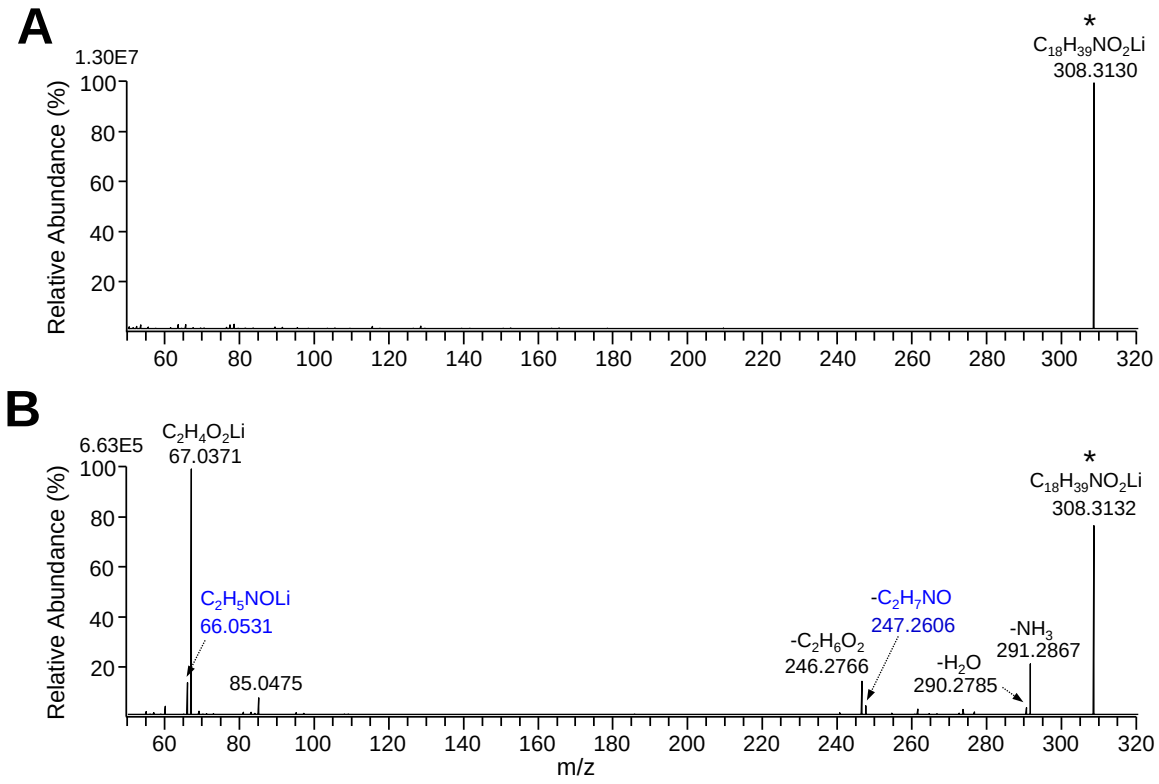

Figure S1. (A) 193 nm UVPD- and (B) HCD-MS/MS of the $[M+Li]^+$ precursor ion of dihydrosphingosine d18:0. Structurally diagnostic sphingosine backbone product ions are indicated in blue text. See Scheme 2 for structural information.

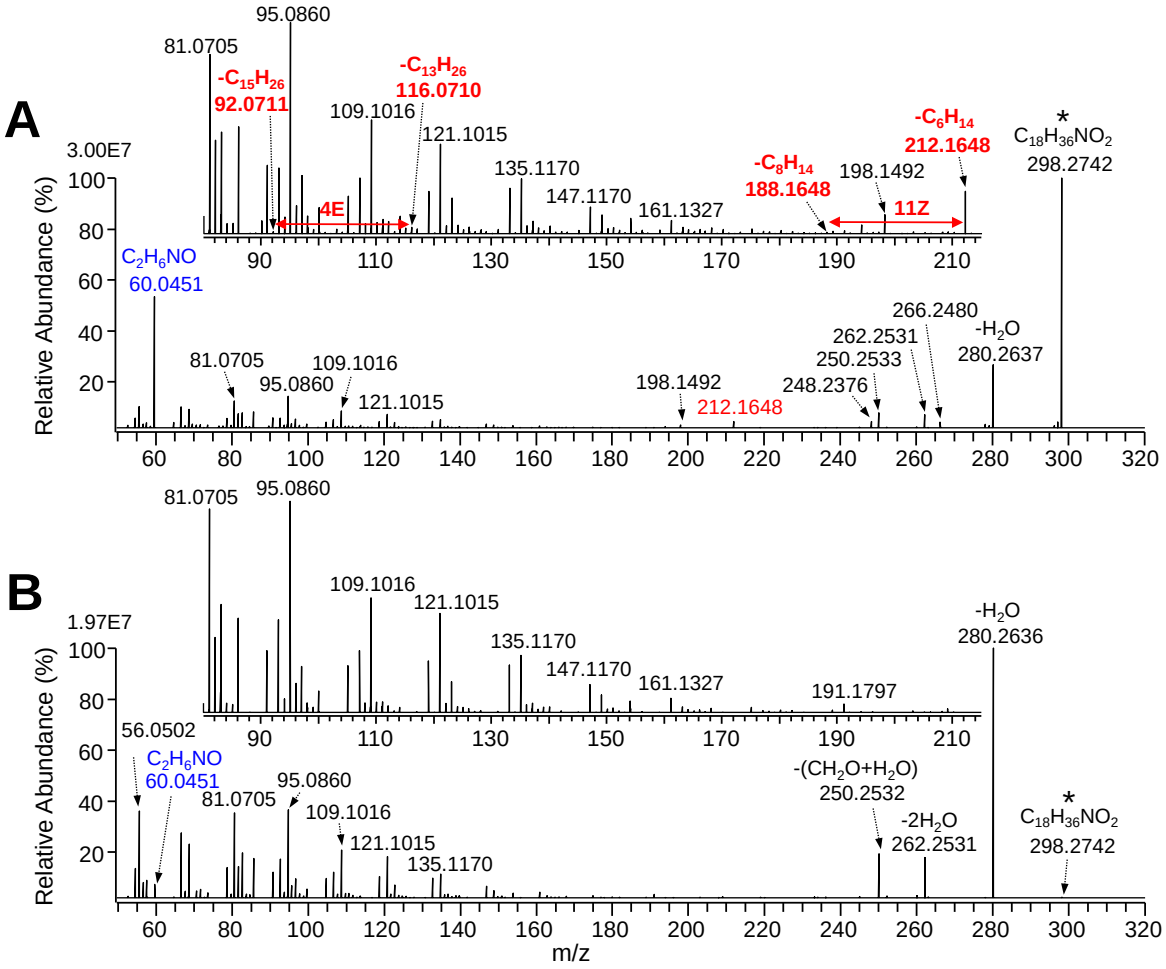

Figure S2. (A) 193nm UVPD- and (B) HCD-MS/MS of the protonated (i.e., $[M+H]^+$) precursor ion of sphingadiene d18:2(4E,11Z). Structurally diagnostic UVPD specific product ions corresponding to cleavage of the sphingosine C=C and alkyl chain C=C double bonds (panel A) are indicated using red text. Structurally diagnostic sphingosine backbone product ions common to both HCD and UVPD are indicated in blue text. See Scheme S2 for structural information.

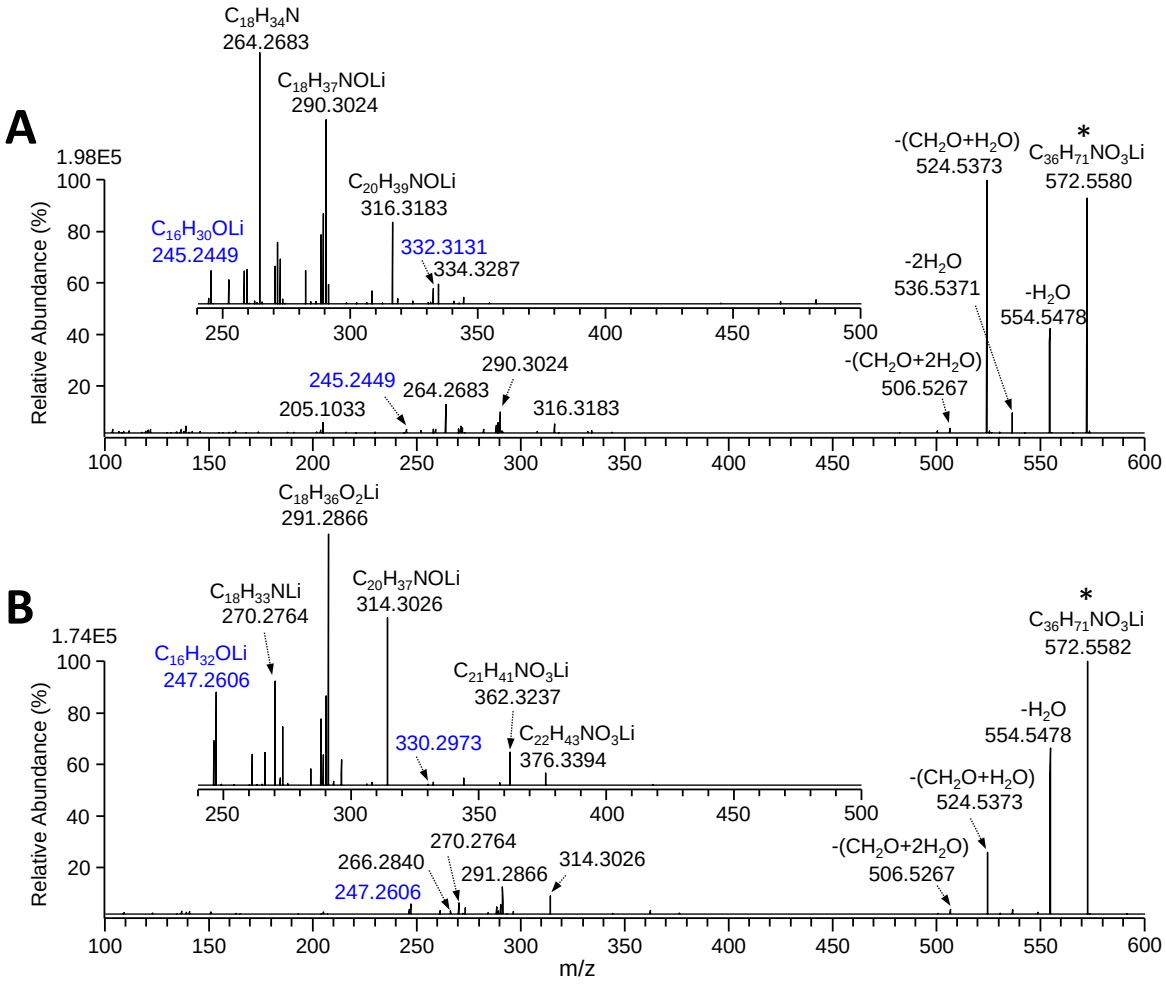

Figure S3. HCD-MS/MS of the $[M+Li]^+$ precursor ions of the isomeric lipid species (A) ceramide d18:1(4E)/18:0 and (B) dihydroceramide d18:0/18:1(9Z). Structurally diagnostic sphingosine backbone product ions common to both HCD and UVPD are indicated in blue text. See Scheme 4 for structural information.

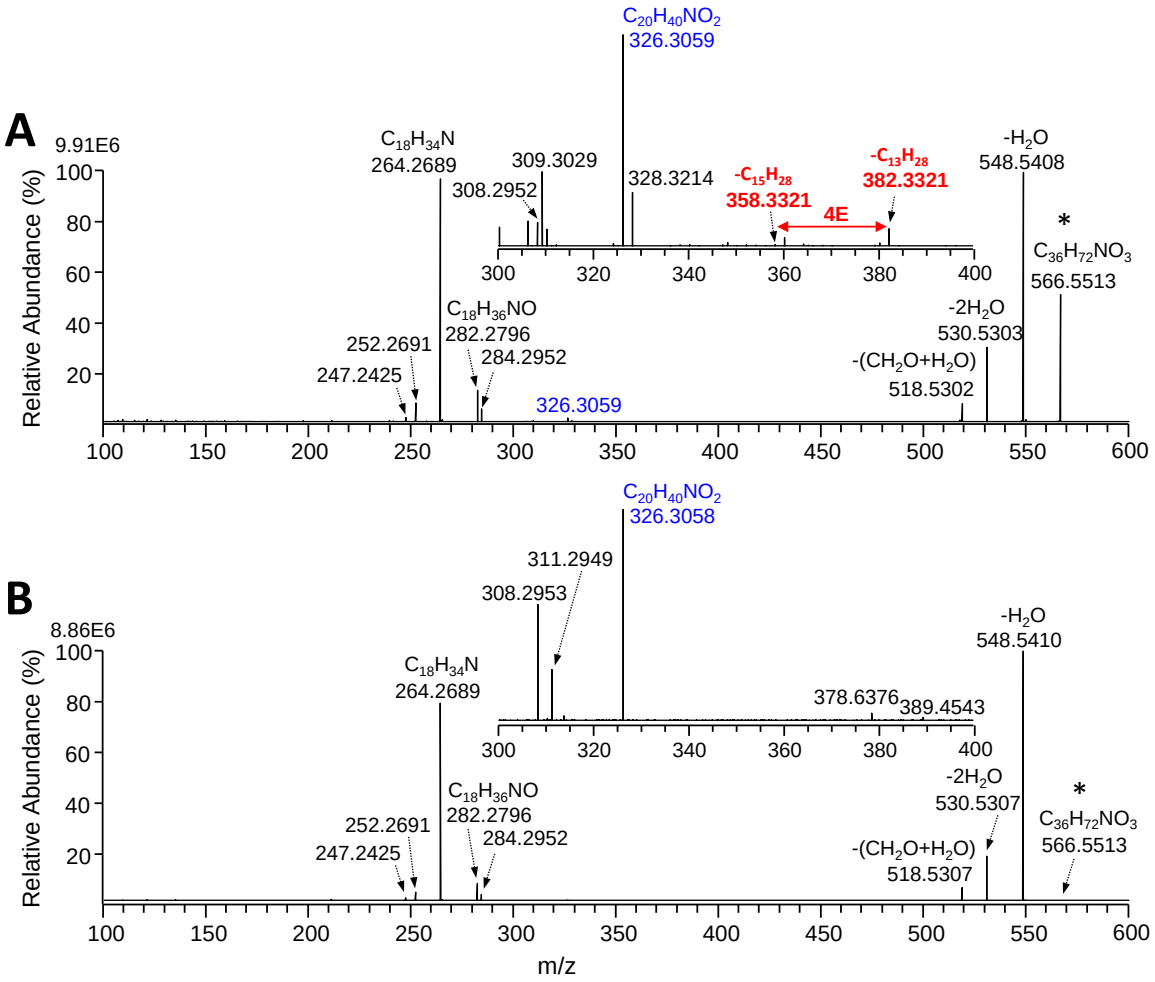

Figure S4. (A) 193 nm UVPD- and (B) HCD-MS/MS of the $[M+H]^+$ precursor ion of ceramide d18:1(4E)/18:0. Structurally diagnostic UVPD specific product ions corresponding to cleavage of the sphingosine C=C (panel A) double bond are indicated using red text. Structurally diagnostic sphingosine backbone product ions common to both HCD and UVPD are indicated in blue text. See Scheme S3 for structural information.

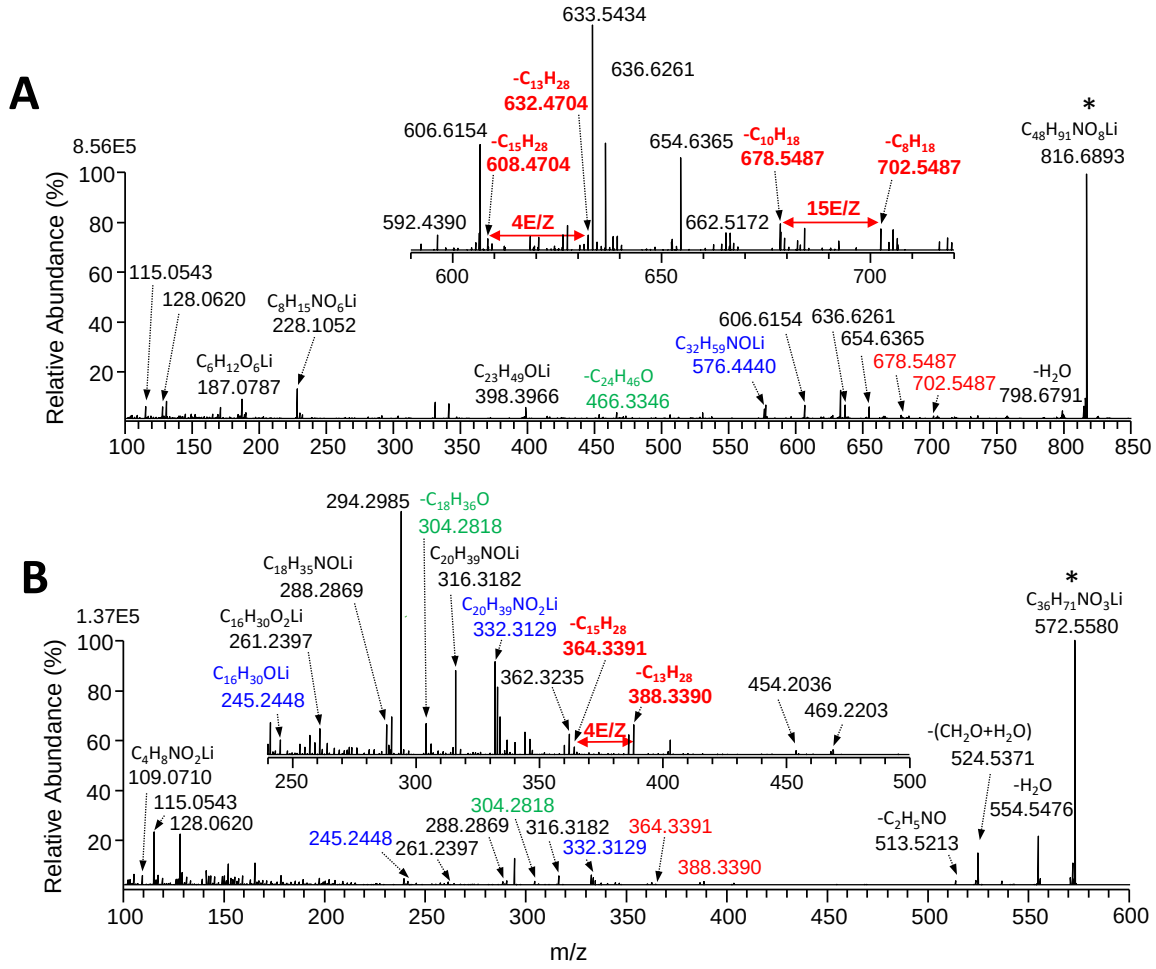

Figure S5. 193 nm UVPD-MS/MS of the $[M+Li]^+$ precursor ions of endogenous lipids (A) hexosyl ceramide d18:1(4E/Z)/24:1(15Z/E) and (B) ceramide d18:1(4E/Z)/18:0 from a porcine brain total lipid extract. Structurally diagnostic UVPD specific product ions corresponding to cleavage of sphingosine C=C and acyl chain C=C double bonds are indicated using red text, while those corresponding to cleavage of the N-C amide bond and sphingosine backbone are indicated using green and blue text, respectively.

Supplemental Schemes

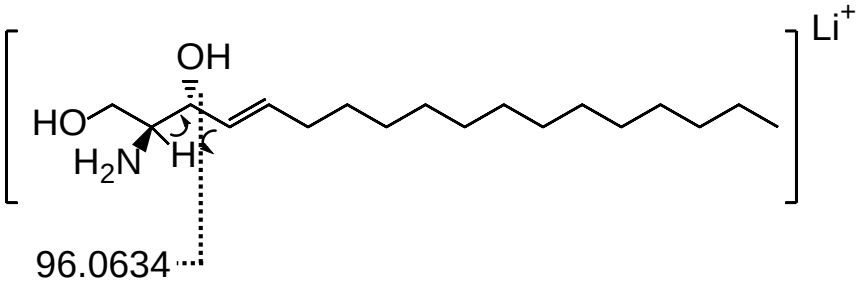

Scheme S1. Proposed mechanism for formation of the m/z 96.0634 ($C_3H_7NO_2Li$) product ion resulting from 193 nm dissociation of the $[M+Li]^+$ precursor ion of sphingosine d18:1.

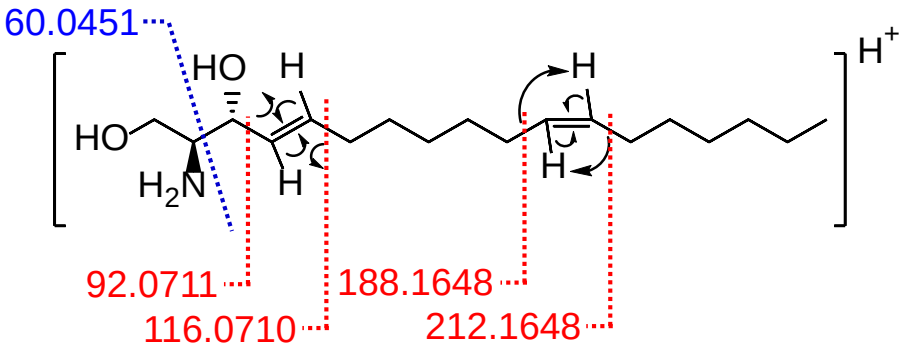

Scheme S2. Summary of the 193 nm UVPD-MS/MS dissociation behaviour of the $[M+H]^+$ precursor ion of sphingadiene d18:2(4E,11Z). Structurally diagnostic UVPD specific product ions corresponding to cleavage of the sphingosine C=C and acyl chain C=C double bonds are indicated using red text, while the structurally diagnostic sphingosine backbone cleavage product ion common to both HCD and UVPD is indicated in blue text. Arrows show the proposed mechanisms for formation of the sphingosine C=C and alkyl chain C=C double bond specific product ions.

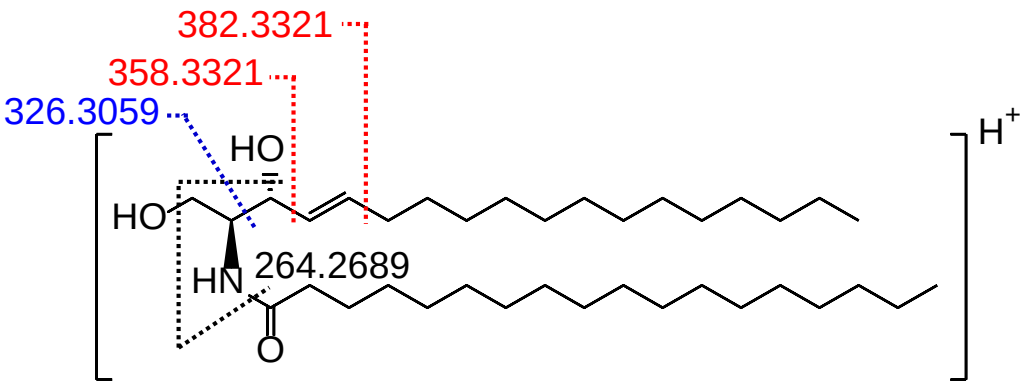

Scheme S3. Summary of the 193 nm UVPD-MS/MS dissociation behaviour of the $[M+H]^+$ precursor ion of ceramide d18:1(4E)/18:0. Structurally diagnostic UVPD specific product ions corresponding to cleavage of the sphingosine C=C double bond are indicated using red text, while the structurally diagnostic sphingosine backbone cleavage product ion common to both HCD and UVPD is indicated in blue text.